Inhibition of Cellular MEK/ERK Signaling Suppresses Murine Papillomavirus Type 1 Replicative Activities and Promotes Tumor Regression

Adrian J. Luna[1,*], Jesse M. Young[1,**], Rosa T. Sterk[1], Virginie Bondu[1], Fred A. Schultz[2], Donna F. Kusewitt[2,4], Huining Kang[3,4], Michelle A. Ozbun[1,4§]

[1] Department of Molecular Genetics & Microbiology, The University of New Mexico School of Medicine, Albuquerque, NM 87131, USA

[2] Department of Pathology, The University of New Mexico School of Medicine, Albuquerque, NM 87131, USA

[3] Department of Internal Medicine, Division of Epidemiology, Biostatistics and Preventive Medicine, The University of New Mexico School of Medicine, Albuquerque, NM 87131, USA

[4] The University of New Mexico Comprehensive Cancer Center, Albuquerque, NMo, USA

*Present address: University of Michigan, Ann Arbor, MI

**Present address: TriCore Reference Laboratories, Albuquerque, NM

§ Corresponding Author

Abstract (300 words)

Human papillomaviruses (HPVs) are a significant public health concern due to their widespread transmission, morbidity, and oncogenic potential. Despite efficacious vaccines, millions of unvaccinated individuals and those with existing infections will develop HPV-related diseases for the next two decades. The continuing burden of HPV-related diseases is exacerbated by the lack of effective therapies or cures for infections, highlighting the need to identify and develop antivirals. The discovery of the mouse papillomavirus type 1 (MmuPV1) and the development of experimental *in vivo* infection models in laboratory mice has provided opportunities to study papillomavirus pathogenesis in cutaneous epithelium, the oral cavity, and the anogenital tract. However, the MmuPV1 infection model has not been used to evaluate potential antivirals. We previously reported that inhibitors of cellular MEK/ERK signaling suppress oncogenic HPV early gene expression *in vitro*. In this report, we adapted the MmuPV1 infection model to determine whether MEK inhibitors have anti-papillomavirus properties *in vivo*. We demonstrate that oral dosage of the MEK1/2 inhibitor trametinib promotes papilloma regression in immunodeficient mice that otherwise would have persistent infections. Moreover, our quantitative histological analyses revealed that inhibition of MEK/ERK signaling reduces E6/E7 mRNAs, MmuPV1 DNA, and L1 protein expression within the MmuPV1-induced lesions. These data suggest that MEK1/2 signaling is essential for both early and late MmuPV1 replication events supporting our previous findings with oncogenic HPVs. We also provide evidence that MEK inhibitors protect from the development of secondary tumors. Thus, our data suggest that MEK inhibitors have potent anti-tumor properties in a preclinical mouse model and merit further investigation as papillomavirus antiviral therapies.

37 **Introduction**

38 Human papillomavirus (HPV) infections are highly prevalent and cause a variety of epithelial neoplasms
39 (i.e., tumors) ranging in severity from benign cutaneous warts to intraepithelial neoplasia to cancers [1].
40 Over 200 HPV genotypes have been identified and sequenced [2] with low-risk mucosotropic HPVs
41 causing 90% of anogenital warts and all laryngeal papillomas and high-risk HPV infections etiologically
42 linked to anogenital and oropharyngeal cancers [3]. Despite effective prophylactic vaccines, millions of
43 unvaccinated people and those with existing infections are projected to develop HPV-related diseases
44 for the next two decades [4]. Current HPV treatments involve lesion excision or ablation, cryotherapy,
45 chemotherapy, and radiation, each risking long-term morbidities with reduced quality of life [5-8].
46 Additionally, recurrence rates can be >50% [9, 10]. To date, there are no effective antiviral HPV therapies
47 and no cure for HPV infections.

48 Like all PVs, HPVs are highly host specific and cannot be productively transmitted to animals. Although
49 this has inhibited detailed studies of HPV pathogenesis and immunology, experimental infections using
50 a variety of vertebrate animal PVs have provided valuable models for understanding viral gene functions,
51 tissue tropism, regression and persistence, cancer progression, vaccine efficacy, and potential
52 therapeutic agents [11]. Despite differences in epithelial tropisms and disease manifestations,
53 mammalian PVs have similar genome organization, protein functions, and reliance on epithelial
54 differentiation for productive replication [1]. The murine PV type 1 (MmuPV1) mouse model is a major
55 advancement in preclinical models of PV-induced infection and disease [12]. However, to our knowledge,
56 this model has not been used to evaluate antiviral agents.

57 In all mammalian PVs tumorigenesis is primarily driven by the E6 and E7 proteins [13, 14]. Although E6
58 and E7 from different PV genera interact with different cellular targets, E6 and E7 expression reprograms
59 cells in the para- and supra-basal layers to maintain cell cycle progression and proliferative capacity [13,
60 15, 16]. This promotes a cellular environment where viral genomes are amplified for packaging by the
61 capsid proteins into new virions [15]. As E6 and E7 proteins are the key factors for PV persistence and

62 oncogenesis, they are ideal therapeutic targets [17, 18]. Genetic knockdown of oncogenic HPV E6 and
63 E7 expression restores cell cycle checkpoint (e.g., p53 and pRb) functions, inhibits cell proliferation, and
64 leads to cellular apoptosis and/or senescence [19-27]. Yet, genetic approaches have not been robustly
65 adaptable to human clinical studies. A handful of small molecules have been investigated for their
66 abilities to inhibit PV protein activities [28], but none so far show promise *in vivo*.

67 We recently reported that cellular MEK/ERK signaling is a key modulator of high-risk HPV E6/E7
68 transcription [29]. The RAS-RAF-MEK-ERK signaling pathway is evolutionarily conserved, has been
69 extensively investigated in mammalian cells, and is the best understood signaling cascade in tumor cell
70 biology [30]. MEK signaling is tightly controlled in normal epithelium where proliferative signals from
71 growth factor receptors are restricted to promote epithelial homeostasis, including cellular contact
72 inhibition and differentiation [31-34]. Thus, MEK signaling is normally limited to the lower epithelial cell
73 layers. MEK signaling is effected by the MEK1 and MEK2 isoforms, which are structurally similar and
74 share activation mechanisms. Upon activation by RAF, they function as dual-specificity tyrosine and
75 serine/threonine kinases, phosphorylating their only known *in vivo* substrates ERK1 and ERK2 on specific
76 tyrosine and threonine residues [35]. MEK1 and MEK2 exhibit extensive functional redundancy and form
77 functional homo- or hetero-dimers *in vivo* [36]. However, increasing evidence suggests that MEK1 and
78 MEK2 have distinct activities that may be controlled by specific modulation of their activity levels [37, 38],
79 differential binding to cellular proteins [39-43] and disparate outcomes when the genes are knocked out
80 in mice [36, 44, 45]. Despite an incomplete understanding of the distinct functions of MEK1 and MEK2,
81 particularly in the epithelium, MEK/ERK activation has long been recognized to play a key role in cell
82 proliferative diseases and neoplastic progression. For example, p-ERK1/2 levels are increased in the
83 upper epithelial layers in several proliferative skin diseases, including HPV-driven cervical neoplasia [46].
84 We found, in a cohort of 580 biopsies from normal cervix, low-, and high-grade cervical intraepithelial
85 neoplasia, a significant correlation ($p<0.001$, $X^2=212.7$) between increasing levels of p-ERK and E7
86 protein activity during disease progression [29]. Mechanistically, using high-risk HPV-infected 3D
87 organotypic (raft) epithelial tissues and monolayer cultures, we showed that MEK-induced

88 phosphorylation of ERK1/2 robustly governs HPV E6/E7 mRNA transcription. Importantly, we
89 demonstrated that small molecule inhibitors of MEK and ERK potently inhibit HPV E6/E7 transcription, at
90 least in part by blocking the activation of AP-1 transcription factors [29] whose binding sites are conserved
91 in the long control region (LCR) enhancer/promoter of all PV genomes [47].

92 The combined conservation of PV genome structure, epithelial differentiation-dependent PV gene
93 regulation, and MEK/ERK signaling in mammalian epithelium prompted us to hypothesize that inhibitors
94 of MEK signaling would suppress E6/E7 gene transcription and tumor growth in the preclinical MmuPV1-
95 induced tumor model that recapitulates key aspects of HPV-induced tumorigenesis [12]. We investigated
96 two FDA- and European Medicines Agency-approved MEK inhibitors, trametinib and cobimetinib [48].
97 Both drugs have similar *in vitro* inhibitory concentration 50 (IC_{50}) efficacies for preventing activation of
98 MEK1 (0.7 nM and 0.95 nM, respectively) and trametinib is equivalently inhibitory of the MEK2 isoform
99 (IC_{50} = 0.9 nM). However, cobimetinib is ≈200-fold less potent against MEK2 (IC_{50} = 199 nM) [48]. After
100 inducing tumors on the tails of Hsd:Athymic-*FoxN1*^{nu} mice that lack T cells, mice were treated orally with
101 drug dosages based on previous studies [48]. Both drugs effectively inhibited tumor growth, but
102 trametinib led to significant tumor regression beginning about 1 week post treatment initiation.
103 Furthermore, the MEK inhibitors prevented overt lesion formation at secondary sites, suggesting
104 diminished MmuPV1 transmission. Both drugs display mechanisms of action consistent with reduced
105 viral gene expression and genome replication and suppressed cellular proliferation as expected from our
106 prior *in vitro* study [29]. Our results show that both MEK1 and MEK2 are important for PV tumorigenesis,
107 and that further investigations of MEK1/2 inhibitors are warranted for the treatment of PV-induced
108 diseases in humans and animals.

109

110

111

112 **Methods**

113 **MmuPV1 infections, tumor growth and treatments.** All animal work was approved by the University
114 of New Mexico's IACUC (protocol # 20-201020-HSC). Female Hsd:Athymic Nude-*Foxn1*^{nu} outbred mice
115 (Envigo) 6-8 weeks of age were inoculated with MmuPV1 virions (a kind gift from Prof. Paul Lambert,
116 Univ. of Wisconsin-Madison). Specifically, the mice were anesthetized and maintained in anesthesia
117 using 3% isoflurane in O_2. Prior to inoculation, the tail of each mouse was scarified using a 27.5-gauge
118 needle. To standardize infection area and papilloma growth the scarification was initiated 0.5-cm distal
119 to the tail base and continuing for 1-cm toward the tip. Each mouse tail was superficially scarified by
120 scratching over the epithelial surface 20-30 times as described [49]. Scarification and viral inoculations
121 were carried out in a biosafety cabinet. MmuPV1 virions ($2x10^8$ viral genome equivalents [VGE] in 2 µl)
122 were applied across the entirety of each wound site using a siliconized pipette tip. The MmuPV1 inocula
123 were allowed to penetrate the wound before returning mice to microisolator (biocontainment) cages. Mice
124 were monitored weekly for weight and the appearance of warts. Tumor volumes were determined with
125 digital calipers (Bel-Art Products) using the formula (length*width*height): length was measured from the
126 sagittal plane, width from the transverse plane, and height was measured from the base to the highest
127 peak. When mice had developed papillomas with a volume of ≥17 mm^3, the animals were stratified by
128 papilloma size and assigned into five groups with similar average tumor volumes (≈40 mm^3). Trametinib
129 (Selleckchem) and Cobimetinib (Selleckchem) in vehicle mixture (30% PEG-300 + 5% DMSO + 5%
130 Tween-80 in dH_2O) were administered by oral gavage and tumor dimensions and body weights were
131 recorded every 48 h. Efficacy was measured as percent tumor growth inhibition (TGI) relative to the
132 vehicle-treated group. TGI was calculated by the equation [1-(*T/C*) x 100], where *T* and *C* represent the
133 mean tumor volumes on day 30 in the MEK inhibitor-treated (T) and vehicle control (C) groups,
134 respectively. A TGI of >50% is considered to be efficacious. On day 30, mice were euthanized by CO_2
135 exposure and whole tail sections receiving the MmuPV1 inoculation were excised to include ≈0.5 cm of
136 uninfected length on each side of the wart growth. Tail sections were fixed in 4% paraformaldehyde (PFA)
137 in PBS overnight at 4°C. Thereafter, each tail section was rinsed twice with sterile PBS and incubated

138 with Versenate decalcifying reagent (StatLab) at 4°C until the tail bone became pliable. Tail sections
139 were rinsed with sterile PBS and stored in 70% ethanol at 4°C until paraffin-embedding. Muzzle
140 papillomas were excised and stored in 4% PFA in PBS overnight before washing twice with PBS and
141 storing in 70% ethanol until paraffin-embedding.

142

143 **MmuPV1 infections *in vitro*.** HaCaT cells were seeded at 10^4 cells per plate in DMEM with 10% fetal
144 calf serum and allowed to adhere overnight at 37°C in 5% CO_2. Cells were pretreated for 1h with medium
145 containing vehicle (0.1% DMSO) or 1.0 to 100 nM trametinib prior to and during MmuPV1 exposure at
146 1000 VGE per cell. Infections proceeded for 48h before harvesting for total DNase I-treated RNA.
147 Following reverse transcription (RT), qPCR was performed using primers to amplify spliced MmuPV1
148 E1^E4 cDNA and normalized to ribosomal protein 18s mRNA levels as previously described [29, 49, 50].

149

150 **Tissue Staining and Immunohistochemistry (IHC).** FFPE tail sections and muzzle specimens 4-5 µm
151 in thickness were baked at 60°C for 1 h. The Ventana Discovery platform was used for deparaffinization,
152 rehydration and H & E staining or blocking of endogenous peroxidases for IHC. Antigens were unmasked
153 by boiling in RiboCC buffer (Ventana 760-107; for keratin 10 and myeloperoxidase) for 32 min at 100°C.
154 Antibodies to cytokeratin 10 (abcam ab76318; 1:250), cytokeratin 5 (abcam ab52635; 1:400), and
155 myeloperoxidase (abcam ab208670; 1:1000) were individually diluted in Discovery PSS Diluent (Ventana
156 760-212), hand applied, and incubated for 16-32 min at 36°C. Antibody incubation was followed by anti-
157 Rb HQ (Ventana 760-4815), anti-HQ HRP (Ventana 760-4820), and DAB CM (Ventana 760-4304)
158 detection. Iimmunohistochemical detection of p-ERK1/2 (Cell Signaling #4370; 1:500) required the
159 tyramide signal amplification (TSA) biotin system following the manufacturer's protocol (AKOYA
160 Biosciences #NEL 700A001KT). Slides were counterstained with hematoxylin (Ventana 760-2021) and
161 Bluing solution (Ventana 760-2037) or with Gill No.1 Hematoxylin solution (Sigma-Aldrich #GHS132-1L)
162 followed by acid alcohol and lithium carbonate rinse. Following dehydration, coverslips were mounted

163 using Permount (Fisher Scientific SP15-500). Stained slides were scanned at 20X using the Leica Versa
164 200 digital slide scanner (Leica Biosystems, Buffalo Grove, IL).

165

166 **DNA and RNA *in situ* hybridization (ISH).** FFPE tail sections were stained according to the
167 RNAscope manufacturer's protocol (2.5 HD Detection Kit-Red, Advanced Cell Diagnostics [ACD]) using
168 probes to detect MmuPV1 E6/E7 RNA (ACD). DNA ISH employed probes to the noncoding MmuPV1
169 LCR Probe (ACD) using the chromogenic DNAscope HD Kit. Slides were counterstained with 50%
170 Gill's hematoxylin solution number 1 (G Biosciences), mounted using EcoMount (BioCare Medical), and
171 digitally imaged as above.

172

173 **Immunofluorescence.** FFPE tail sections were deparaffinized, rehydrated, and subjected to heat-
174 induced antigen retrieval for 30 min using pH 9 target retrieval solution (Dako). Endogenous
175 peroxidases were blocked with 3% hydrogen peroxide in methanol for 10 min. Tissues were blocked
176 with 5% goat serum in PBS containing 0.1% Tween-20 (PBS-T) for 1 h at room temperature, then
177 incubated at 4°C overnight with rabbit sera against MmuPV1 L1 (a kind gift form Chris Buck, NIH;
178 1:2500) and chicken anti-keratin 14 (BioLegend 905301; 1:500) diluted in 5% goat serum in PBS-T.
179 The sections were then washed three times in PBS-T followed by incubation with secondary antibodies
180 (1:500) AF488 goat anti-rabbit IgG (ThermoFisher A32731) and AF647 goat anti-chicken IgG
181 (ThermoFisher A32933) for 1 h at room temperature. Coverslips were mounted using ProLong
182 Diamond Antifade DAPI Mountant (Thermo Fisher). Images were acquired using a Leica TCS SP8
183 confocal microscope with fixed data acquisition settings. L1-positive foci were counted using Huygens
184 essential software object analysis tool (Scientific Volume Imaging, The Netherlands, http://svi.nl).

185

186 **Morphometric Tissue Analysis.** Tissue morphometry was performed on digitally acquired images
187 from all tumors using HALO software (Indica, Albuquerque, NM), under the supervision of a board-
188 certified veterinary pathologist (Kusewitt). The thickness of the epithelium within each lesion was
189 determined using H&E sections. The linear length of the lesion was measured, and HALO was trained
190 to recognize all epithelial elements lying above the dermis, then the area of epithelium within the lesion
191 was determined. The epithelium within each region was selected using the bucket tool; the selection
192 was refined using the line and scissors tools to include all nucleated cells and to eliminate artifacts.
193 Within the identified epithelium, stroma was identified and eliminated from consideration. Epithelial
194 thickness was expressed as the ratio of epithelial area to lesion length (mm). Using the CytoNuclear
195 algorithm, individual epithelial cells were identified and cytoplasmic staining for each marker was
196 categorized as negative, low, medium, or high. The total number of cells examined was enumerated
197 and the percentage of epithelial cells staining at each intensity was determined (e.g., *SI Appendix* Fig.
198 S3A-C). As the ISH staining lacked sufficient nuclear demacation, total areas positive for ISH signals
199 were determined. Neutrophil infiltration was quantified by selecting all lesional epithelium and
200 underlying dermis by hand. The percentage of that area occupied by myeloperoxidase-positive
201 neutrophils was determined using HALO software to identify and quantify the area of positive staining.
202 IHC stained slides were excluded from analysis (no more than one per treatment group) if they lacked
203 clear evidence of tail features that ensured the tumor was adequately represented.

204

205 **Statistical Analyses**. Morphometry analyses included data from 5-6 tumors per group subjected to
206 one-way analysis of variance (ANOVA) with Tukey's multiple comparison test. RT-qPCR data were
207 analyzed by one-way ANOVA with Dunnett's multiple comparisons test. Biomarker level correlation
208 coefficients (r) were calculated from morphometry data using Pearson's correlation analysis and
209 computing a two-tailed p value. Tumor measurements among the five treatment groups were analyzed
210 at each time point using the generalized least square (GLS) method to account for the unequal
211 variances among the groups (*SI Appendix* Table 1). Differences among tumor groups at 30 days post

212 treatment were evaluated by ANOVA with the Tukey HSD (honest significant difference) pairwise
213 comparisons (*SI Appendix* Table 2). The rates of tumor volume changes were estimated and
214 compared using the linear mixed-effects model (LMM) analysis (*SI Appendix* Tables 3 and 4).

215

216 **Results**

217 **MEK Inhibitors Suppress MmuPV1-Induced Tumor Growth and Reduce Papillomatous**
218 **Morphology.** After MmuPV1 inoculation and 6 weeks of papilloma growth, mice were randomized into
219 treatment groups; the average tumor volume of each group was ≈40 mm^3 (Fig. 1A) with no significant
220 size differences among the groups (*SI Appendix* Table 1). Mice were orally administered either vehicle,
221 the MEK1 inhibitor cobimetinib (7.5 mg/kg or 15 mg/kg), or the MEK1/2 inhibitor trametinib (1.0 mg/kg or
222 2.0 mg/kg) every 2 days. As visualized in Fig. 1B, C and detailed in *SI Appendix* Table 1, tumor volumes
223 significantly differed among the five groups after 8 days of treatment ($p=0.042$) and the difference became
224 increasingly pronounced as time passed. Over the 30-day treatment period, tumors of vehicle-treated
225 mice increased in size by an average of 2.59-fold, resulting in a final average tumor volume of 101.7
226 mm^3. Comparatively, mice treated with 7.5 mg/kg or 15 mg/kg of cobimetinib demonstrated significantly
227 impaired papilloma growth resulting in final average tumor volumes of 42.4 mm^3 (58% TGI) and 45.4 mm^3
228 (55% TGI), respectively. More strikingly, trametinib treatment resulted in papilloma regression over the
229 same period, reducing tumor volumes to an average of 25.0 mm^3 for 1 mg/kg trametinib and 25.2 mm^3
230 for 2 mg/kg trametinib (both 75% TGI). Pairwise comparisons revealed significant differences between
231 vehicle-treated and each of the drug treatment groups (adjusted p-value <0.05), but no significant
232 differences when comparing each of the four groups that received the MEK inhibitors (*SI Appendix* Table
233 2). Similarly, the rates of tumor volume change (mm^3/day) among the treatment groups estimated by
234 linear mixed-effects model analysis showed that the vehicle-treatment group significantly increased over
235 time while the trametinib-treated groups significantly decreased, and the cobimetinib-treated groups did
236 not have a significant change (*SI Appendix* Table 3). Furthermore, trametinib demonstrated significant

237 superiority over cobimetinib in promoting tumor regression as demonstrated by comparing the rates of
238 tumor volume change among the MEK inhibitor treated groups (p-value = 0.0334; *SI Appendix* Table 4).
239 The visual characteristics of the tail papillomas on mice treated with MEK inhibitors were distinct
240 compared to papillomas on vehicle-treated mice (Fig. 1D; *SI Appendix* Fig. S1). Specifically, vehicle-
241 treated mice bore florid and irregular papillomas. Whereas mice treated with both cobimetinib doses
242 exhibited smaller tumors with less florid appearance, mice treated with both trametinib doses generally
243 displayed more flattened and smoother papillomas (Fig. 1D; *SI Appendix* Fig. S1). Note that only one
244 animal, in the high dose trametinib treatment group, showed significant weight loss suggesting toxicity
245 (*SI Appendix* Fig. S1F-H). These data indicate that MEK inhibitors have profound TGI effects *in vivo* using
246 the MmuPV1 preclinical model; compared to the MEK1 inhibitor cobimetinib, the MEK1/2 inhibitor
247 trametinib, demonstrated superior TGI.

248

249 **MEK Inhibitor Effects on Tissue Morphology and Cellular Biomarkers.** Serial sagittally-sectioned
250 tails were analyzed histologically after H&E staining, focusing on the mice treated with vehicle and those
251 treated with the higher doses of the two MEK inhibitors (Fig. 2A; *SI Appendix* Fig. S2). Papillomas from
252 vehicle-treated mice showed extensive fibrillary projections throughout the tumor cross-sections. In drug-
253 treated mice, particularly those treated with the MEK1/2 inhibitor, the extent of papillary projections was
254 considerably reduced (Fig. 2A). Consistent with this observation, morphometric analyses of all tumors
255 revealed significantly reduced epithelial thickness in the papillomas from mice treated with the MEK
256 inhibitors compared to vehicle-treated mice (Fig. 2B). Tumor sections from all three groups revealed
257 dysplastic epithelium and hyperkeratosis, albeit with noticeable differences depending upon the
258 treatment (*SI Appendix* Fig. S2). Koilocytes, epithelial cells characterized by perinuclear haloes
259 (cytoplasmic vacuolation) surrounding condensed nuclei, are pathognomonic of HPV infections [51] and
260 were scattered irregularly throughout the differentiating epithelium in all MmuPV1 lesions.

261 The MEK inhibitors suppressed the levels of phosphorylated-ERK1/2 (p-ERK1/2), the only recognized
262 signaling effector of MEK, in the tumors (Fig. 2C-D); moreover, p-ERK1/2 levels correlated significantly
263 with tumoral epithelial lesion thickness (p=0.00185; *SI Appendix* Fig. S5A). p-ERK1/2 was most
264 prominent in the papillomas of vehicle-treated mice, localizing primarily to basal and lower suprabasal
265 layers of all papillomas. These data indicate that the systemically delivered MEK inhibitors reached the
266 tail epithelium to suppress MEK/ERK signaling. Further, the findings suggest that MEK signaling is an
267 important contributor to papilloma growth and maintenance in the MmuPV1 mouse model.

268 As MEK/ERK signaling is integral to epithelial proliferation and differentiation [52], we evaluated the
269 papillomas for differentiation-associated epithelial markers, keratin 5 (K5) and keratin 10 (K10). K5 pairs
270 with K14 and these proteins are characteristic of mitotically active, undifferentiated basal cells of the
271 epithelium; their expression is downregulated as cells begin to differentiate [53]. In contrast, K10 is an
272 established early marker of keratinocytes entering terminal differentiation [54]. As expected, strong K5
273 staining was prominent in the cells nearest the basement membranes of all tumors. The vehicle-treated
274 mice displayed an expansive network of undifferentiated cells throughout the thickness of the fibrillary
275 papillomas (Fig. 2E; *SI Appendix* Fig. S3A-D), as previously reported for MmuPV1 tail lesions [16].
276 However, MEK inhibitors counteracted basal cell expansion and the number of K5-positive cells was
277 reduced (Fig. 2F) and correlated significantly with both p-ERK1/2 levels (p=0.0249) and lesion thickness
278 (p=0.000569; *SI Appendix* Fig. S5B-C, respectively). Likewise, the number of differentiating K10-positive
279 cells was significantly lower in the smaller papillomatous lesions of the drug-treated mice compared to
280 those in vehicle-treated mice (Fig. 2G-H). Interestingly, there were no significant differences amongst the
281 treatment groups in the percentages of lesional cells that expressed p-ERK1/2, K5, or K10 (*SI Appendix*
282 Fig. S3E-G). These findings indicate that while MEK inhibition and suppressed p-ERK1/2 signaling
283 reduced the number of proliferative cells, there were no net changes in the overall proportion of cells
284 proliferating or differentiating within the papillomas.

285 Infection with MmuPV1 or oncogenic HPVs leads to increased expression of Ki67, a basal cell
286 proliferation marker [55-58] and Sundberg et al. showed similar staining patterns between Ki67 and K5

287 in MmuPV1-induced tail tumors [55]. Furthermore, MEK inhibition is known to reduce Ki67 staining in
288 epithelial tumors [59, 60]. Although we attempted to detect Ki67 by IHC in the tumor sections, we were
289 unable to obtain robust and quantifiable Ki67 staining (data not shown). This is likely because tissue
290 decalcification has been found to impair the detection of nuclear biomarkers [61].

291

292 **MEK Inhibitor-Induced Papilloma Regression does not Involve T Cells or Neutrophils.** Whereas
293 various data indicate that CD4+ and CD8+ T cells play a major role in papillomavirus-induced lesion
294 regression [55, 62-65], there also are indications that neutrophils might contribute to MmuPV1 disease
295 control in immunocompetent models [66]. As the Hsd:Athymic-*FoxN1*^{nu} mice used in this investigation
296 lack CD4+ and CD8+ T cells but have an intact innate immune system, we investigated if MEK inhibition
297 resulted in increased neutrophil infiltration in the MmuPV1-induced papillomas. Quantification of tumor-
298 proximal myeloperoxidase staining revealed no significant differences in neutrophil infiltration amongst
299 treated and control papillomas (Fig. 3A-B). Thus, the data suggest that MEK inhibitors suppressed tumor
300 growth and trametinib caused regression *via* a mechanism independent of T cells and neutrophils.

301

302 **The MmuPV1 Vegetative Replication Cycle is Dependent on MEK Signaling.** Our recent publication
303 demonstrated that HPV early gene expression relies on MEK/ERK signaling and that MEK1/2 inhibition
304 results in reduced viral early gene transcription and protein expression [29]. As robust PV genome
305 amplification leading to late gene expression depends on sufficient PV early gene expression [67], we
306 determined the effect of MEK inhibition on key aspects of the complete MmuPV1 replicative cycle. We
307 first strove to quantify the tumor levels of E6/E7 oncogene mRNA, which should be present predominantly
308 in the cytoplasm of infected epithelium (Fig. 3C). Despite various DNase treatment methods to remove
309 viral genomes, the E6/E7 probes consistently bound to nuclear targets, particularly evident in the vehicle-
310 only tumors (*SI Appendix* Fig. S4A). Thus, the data in Fig. 3C-D likely represent detection of MmuPV1
311 genomes and E6/E7 mRNAs; yet the morphometric analyses demonstrate the MEK inhibitors significantly

312 reduced the levels of MmuPV1 nucleic acids in the tumors. Consistent with this interpretation, the ISH
313 probe specific to the MmuPV1 noncoding long control region (LCR), revealed ISH staining patterns with
314 obvious overlap in serial sections (Fig. 3, compare panels C and E; *SI Appendix* Fig. S4). Morphometric
315 quantification of ISH data showed overall lower levels of LCR-targeted viral genomes compared to the
316 E6/E7 ISH results in each treatment group (Fig. 3F and D, respectively). There was a highly significant
317 correlation between E6/E7 ISH and LCR ISH ($p<0.00001$; *SI Appendix* Fig. S5J). Furthermore, both
318 RNA ISH and DNA ISH levels correlated strongly with p-ERK1/2 levels ($p<0.001$; *SI Appendix* Fig. S5E-
319 F). Together, the data indicate significantly decreased viral genome levels and imply reduced E6/E7
320 mRNAs in tumors from mice receiving the MEK inhibitors. Lastly, IF detection of MmuPV1 major capsid
321 protein L1 along with K14 staining of undifferentiated basal cells in the tumor sections revealed
322 significantly fewer L1-positive foci in the differentiating layers of tumors of the cobimetinib and trametinib
323 treatment groups (Fig. 3G,H). Additionally, viral LCR and E6/E7 ISH correlated strongly with detected L1-
324 foci ($p<0.0015$ and $p<.000001$; *SI Appendix* Fig. S5L-M). These data strongly support the idea that the
325 MEK inhibitors suppressed the MmuPV1 replicative cycle *in vivo*.

326

327 **MEK Inhibitor Treatment Reduces MmuPV1 Transmission *in vivo.*** Over the treatment course, we
328 observed that all (6/6) vehicle-treated mice developed papillomas on their muzzles (Fig. 4A; Table 1). In
329 contrast, the only mouse from the MEK inhibitor treatment cohorts to develop a visible facial wart (1/24)
330 was in the group receiving the lower dose (7.5 mg/kg) of cobimetinib (Table 1). This mouse was co-
331 housed with other animals receiving cobimetinib (i.e., it was not co-housed with vehicle-treated mice).
332 H&E staining and E6/E7 ISH confirmed that the facial lesions arose from MmuPV1 infections (Figure 4B).
333 As the snouts were not experimentally scarified or infected, the secondary muzzle-arising infections were
334 likely transmitted from tail grooming. The most obvious explanation for lack of secondary muzzle
335 infections in MEK inhibitor-treated mice is that their tail papillomas produced fewer virions due to
336 suppressed viral replication as shown in Fig. 3C-H. We reported that MEK/ERK signaling stimulates HPV
337 early gene expression *via* activation of cellular fos/jun family transcription factors [29], which bind to AP-

338 1 factor binding sites that are highly conserved in papillomavirus LCRs [68]. Thus, it is also possible that
339 MEK inhibition would result in lower viral early gene transcription after infection-mediated delivery of viral
340 genomes to the cell nucleus. To test this prospect, we exposed HaCaT keratinocytes to MmuPV1 virions
341 in the presence of increasing doses of trametinib. Indeed, MEK inhibition resulted in significantly
342 decreased levels of spliced MmuPV1 E1^E4 mRNAs compared to vehicle treated cells (Fig. 4C).
343 Combined, our data suggest that MEK inhibition is likely to impede new MmuPV1 infections by both
344 reducing virion shedding from existing lesions and by suppressing early viral transcription during infection
345 establishment at new sites.

346

347

348 **Discussion**

349 Herein we demonstrate the potent antiviral and tumor suppressive properties of MEK1/2 inhibitors in a
350 preclinical model of HPV disease. To our knowledge, this is the first report to assess antiviral candidates
351 in the MmuPV1 preclinical model. This work confirms and extends our recent study showing that
352 inhibiting MEK/ERK signaling has antiviral effects, specifically reducing early gene transcription and
353 oncoprotein functions, against oncogenic HPVs in three dimensional organotypic epithelial tissue cultures
354 [29]. The conservation of MEK/ERK signaling in mammalian epithelium coupled with the conservation of
355 MEK/ERK activated AP-1 transcription factor binding sites in the LCRs of animal PVs indicates that this
356 pathway is both critical for controlling PV early gene transcription and a prime target for PV antivirals.
357 Thus, our work suggests that targeting this pathway will have antiviral effects for all mammalian PV
358 infections. Importantly, in our prior work and in this study, the antiviral and tumor suppressive effects of
359 MEK inhibitors on PV infections occurred in the absence of T cells, which has critical implications for
360 treating PV infections in individuals lacking functional T cells.

361 A major strength of this study is the use of pathologist-guided, quantitative tumor tissue analyses of tumor
362 thickness and a battery of biomarkers relevant to PV-induced tumorigenesis. Coupled to robust statistical
363 analyses, our objective quantification of biomarkers revealed clearly that MEK inhibitors accessed the
364 epithelium to suppress p-ERK1/2 levels, basal cell expansion, and tumor thickness without affecting
365 overall epithelial differentiation. Whereas it is most likely that MEK inhibition suppressed tumor growth
366 *via* both blunting ERK-mediated cellular proliferative signals and reducing MmuPV1 early gene
367 transcription leading to cell proliferation, the precise contribution of each of these interdependent activities
368 to the overall decreased tumor growth will be challenging to dissect. To our knowledge this is the first
369 study to use quantitative histological analyses of PV-induced pathology.

370 The MmuPV1 tumor growth inhibitory effect of the MEK1/2 inhibitor, trametinib, was superior to that of
371 cobimetinib, which preferentially targets the MEK1 isoform. Despite the functional redundance of MEK1
372 and MEK2 in many assays [36], our understanding of their distinct activities and differential regulation is
373 expanding. For example, MEK1 contains a site (Thr292) for ERK-mediated feedback phosphorylation;
374 MEK2 lacks this site [37, 38]. Additionally, several scaffold proteins specifically bind to and enhance the
375 activation of MEK1, but not MEK2 [39-42]. MEK1 knockout in mice is embryonic lethal [36, 44], whereas
376 MEK2 knockout animals are viable, fertile, and phenotypically normal [45]. MEK2, but not MEK1,
377 phosphorylates the tumor suppressor GCIP (Grap2- and cyclin D1-interacting protein), promotes its
378 degradation, and decreases its tumor suppressor function [43]. Our work suggests that inhibition of both
379 MEK1 and MEK2 is crucial for controlling PV disease. However, MEK2 has distinct functions important
380 for MmuPV1 tumor growththat will require futher dissection. .

381 The tumor suppressive properties of MEK1/2 inhibition by trametinib became evident only four days post
382 treatment, when the mean tumor volumes in the drug-treated groups were smaller than the group's mean
383 starting tumor volumes (Fig. 1C, *SI Table 1*). While the tumors in the trametinib-treated groups continued
384 to decrease in size over the next two weeks, the growth reduction seemed to plateau thereafter. This
385 raises the question as to whether continued trametinib treatment would eventually cure the infections, or
386 whether the drug had reached its maximum effects. It seems likely that ceasing treatment with the drugs

387 prior to complete MmuPV1 clearance would result in regrowth of the tumors, but this has yet to be tested
388 and it would also be useful to do so in the context of functional T cells.

389 The mechanisms by which the MEK inhibitors exerted their effects in this MmuPV1 infection and
390 tumorigenesis model are consistent, in part, with those observed in other non-PV-related cancer models.
391 In a variety of cancer cell types *in vitro*, trametinib and cobimetinib have been shown to reduce p-ERK1/2,
392 modulate cyclin D1 and p27 levels in a manner aligned with a G1/S cell cycle arrest, and induce caspase-
393 dependent apoptosis [60, 69, 70]. Unfortunately, a limitation of our study wss the inability to detect
394 nuclear antigens in the lesions due to Versenate treatment of the tails before fixation. Because Sundberg
395 et al. showed similar staining patterns between Ki67 and K5 in MmuPV1-induced tail tumors [55], and we
396 found a significant correlation between p-ERK1/2 levels and strong K5 staining (p=0.025; Fig. S5B), we
397 infer that MEK inhibitors suppressed cellular proliferation. Additionally, the highly significant correlations
398 between p-ERK1/2 levels and MmuPV1 E6/E7 mRNA (p= 6.85e-5) and between strong K5 staining and
399 MmuPV1 E6/E7 mRNA (p= 9.995e-5) highlight the interdependency of the biomarkers p-ERK1/2, K5 and
400 MmuPV1 E6/E7 mRNA transcription (Fig. S5B, E, I). Future studies evaluating markers of proliferation,
401 apoptosis, and senescence will be needed to clearly delineate the antiproliferative effect of MEK inhibition
402 in mammalian PV tumors.

403 In our previous study and in this work, the antiviral and tumor suppressive effects of MEK inhibition
404 occurred in the absence of T cells [29]. This has important clinical implications for treating PV diseases
405 in those who are immunocompromised [71]. For example, people living with AIDS have increased HPV
406 acquisition, prevalence, persistence, high tumor burdens, and cancer progression [72] and would greatly
407 benefit from effective HPV antiviral treatments. Herein, neither T cells nor neutrophils were implicated
408 tumor regression despite reports that immune mediated cell death is an important characteristic of tumor
409 reduction (reviewed in [73]). Whether immune cell populations are involved in the MEK-inhibitor induced
410 regression of PV neoplasia will require further investigation. Importantly, use of MEK1/2 inhibitors as a
411 therapeutic for PV diseases must be tested in the context of functional T cells as MEK signaling is induced
412 by T cell receptor signaling [74]. While this could be a disadvantage to tumor clearance, recent evidence

413 indicates that MEK inhibitors can lead to a shift from a Th2 to a Th1 response [75], a reduction of
414 regulatory T cells (Tregs) [76], and reprogramming of CD8+ T cells into memory stem cells with antitumor
415 activities [77]. Lastly, we provide strong evidence that MEK inhibitors reduced productive MmuPV1
416 infection measured by both the reduced levels of the viral capsid protein, L1 in tumors, and the lack of
417 secondary muzzle infections observed in the MEK inhibitor-treated mice. In total, our work suggests that
418 MEK1/2 inhibitors warrant further investigation for treatment of mammalian PV infections *in vivo*; such an
419 approach might also reduce PV transmission to new susceptible epithelial sites or between individuals.

420

421

422 **Acknowledgements**

423 This study was supported by the American Cancer Society Mission Boost Grant MBG-18-207-01-COUN
424 (M.A.O.); and the US National Institutes of Health Grants: R21DE028652 (M.A.O.); T32AI07538,
425 F31CA232536, UNMCCC Matching Support (A.J.L.); P30CA118100 (M.A.O.). We acknowledge support
426 by the following University of New Mexico Comprehensive Cancer Center shared resources (NCI
427 2P30CA118100): Human Tissue Repository and Tissue Analysis, Animal Models, Biostatistics.

428 We are grateful to Dr. Paul Lambert and members of his lab for generously providing infectious stocks of
429 MmuPV1, to Dr. Nagayasu Egawa for sharing his protocols for mouse tail scarification and infection, and
430 Dr. Christopher Buck for sharing his rabbit sera against MmuPV1 L1.

431

432

433 FIGURES

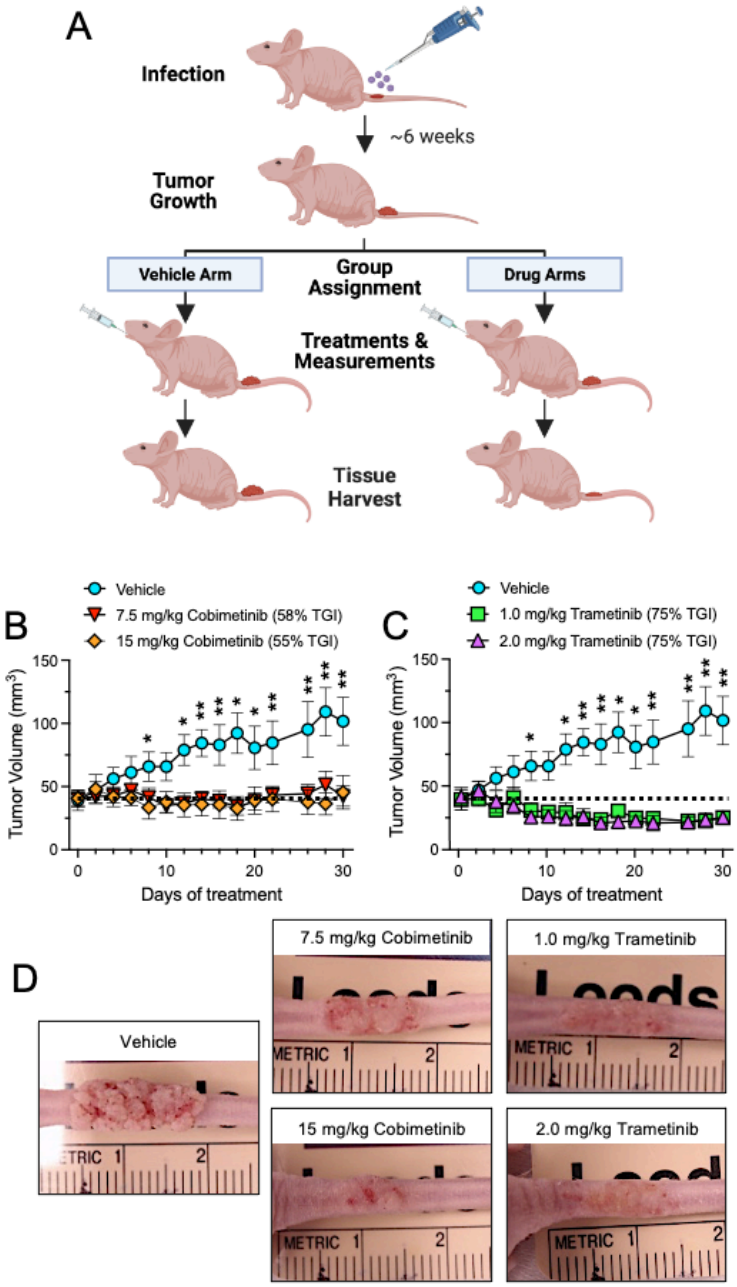

434

435 **Figure 1. MEK inhibition impairs MmuPV1-induced papilloma growth.** (A) Immediately after epithelial tail
436 scarification, female Hsd:Athymic Nude-*Foxn1*^{nu} mice were exposed to $2x10^8$ vge of MmuPV1. Papillomas were
437 allowed to grow for 6 weeks before assigning the animals into vehicle or treatment groups with similar average
438 tumor volumes (n=6 animals per group). Mice were treated by oral gavage treatment every 48h before harvesting
439 the tumor-bearing tail sections on day 30 post treatment. Image created with BioRender.com. (B, C) Mean tumor
440 volumes tracked over the treatment period with (B) cobimetinib or (C) trametinib (the vehicle group was the same
441 for both drugs). The dotted horizontal line marks the mean starting volumes. Data were analyzed comparing all
442 treatment groups together using ANOVA with the generalized least square method (*p<0.05 and **p<0.01; *SI*
443 *Table 1*); the treatments were graphed separately for clarity. Error bars represent SE. Mean TGI for the MEK
444 inhibitors were 58% and 55% for the 7.5 mg/kg and 15 mg/kg cobimetinib, respectively and 75% for both doses of
445 trametinib. (D) Representative images of the MmuPV1 induced papillomas for each treatment group at day 30
446 post treatment initiation.

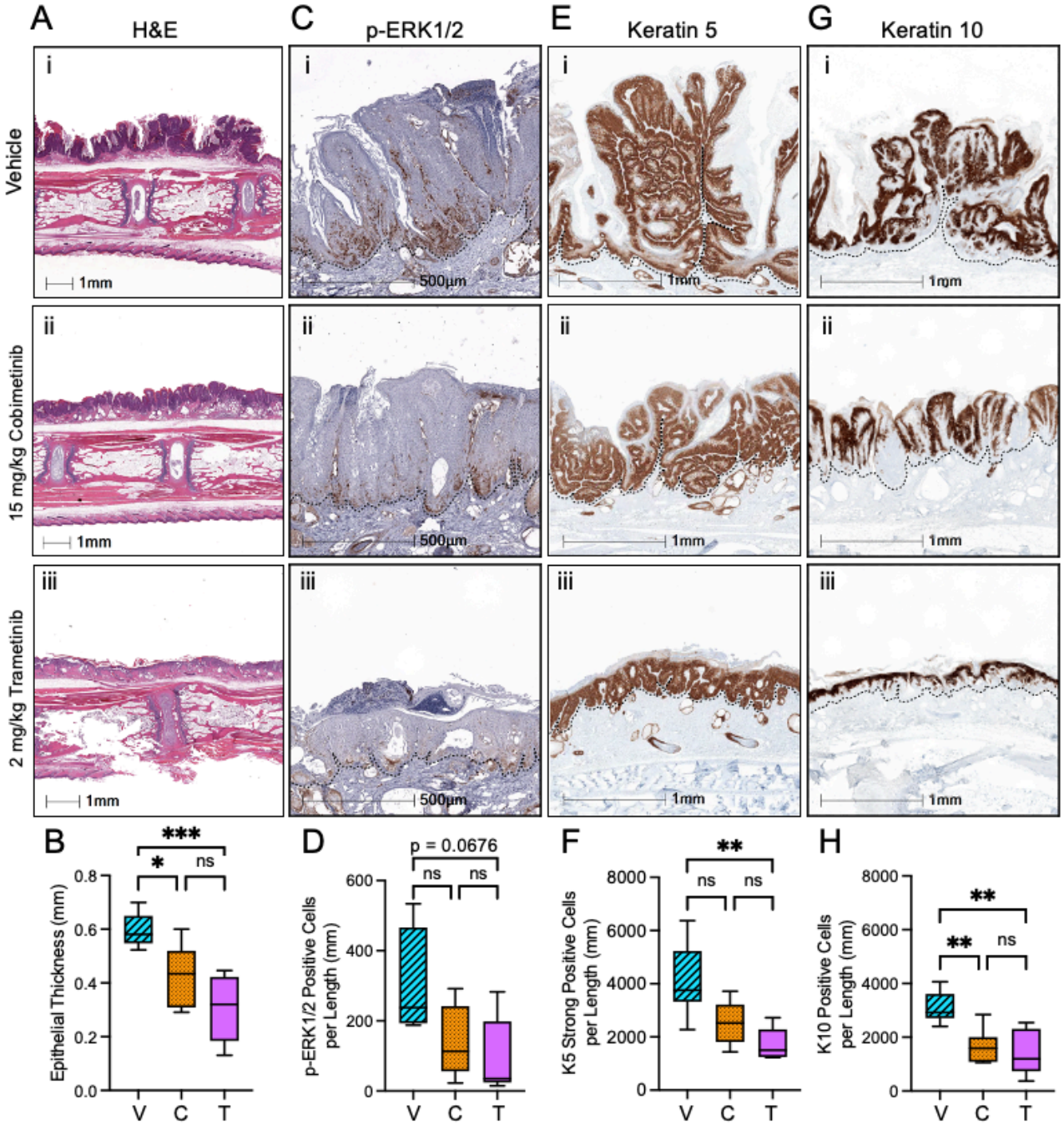

Figure 2. Histological and immunohistochemical analysis of MmuPV1-induced papillomas. Representative images of papilloma histology from mice treated with vehicle (i),15 mg/kg cobimetinib (ii), or 2.0 mg/kg trametinib (iii). Tails were fixed with paraformaldehyde, paraffin embedded, sectioned, and stained: (A) H&E; (C) IHC for p-ERK1/2; (E) IHC for keratin 5 (K5); (G) IHC for keratin 10 (K10); dotted lines mark the basement membrane. (B, D, F, H) Morphometric quantification of tail tumors from each mouse (4-5 per group) for papilloma thickness (height, B); p-ERK1/2 (D), K5 (F), and K10 (H) IHC staining expressed as positive cells per tumor length (mm); vehicle (V), 15 mg/ml cobimetinib (C), 2.0 mg/kg trametinib (T). Data were analyzed using one-way ANOVA with Tukey's multiple comparison test (*p<0.05, **p<0.01; ***p<0.001).

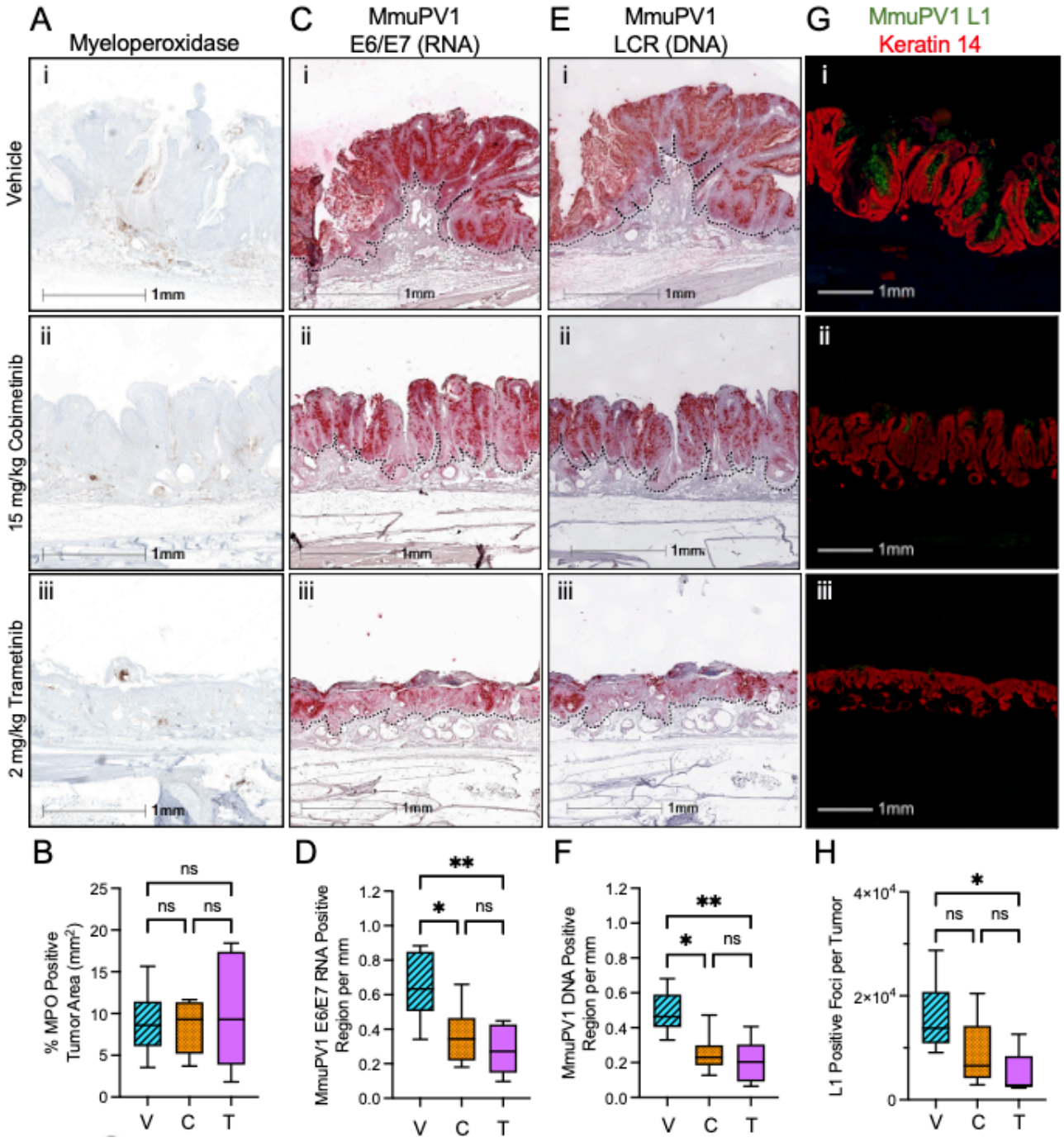

Figure 3. Histological analysis of immune and viral markers in MmuPV1-induced papillomas. Representative images of fixed histological papilloma sections for mice treated with vehicle (i),15 mg/kg cobimetinib (ii), or 2.0 mg/kg trametinib (iii). Tissues were stained *via*: (A) IHC for neutrophil marker, myeloperoxidase (MPO); (C) ISH for MmuPV1 E6/E7 mRNA; (E) ISH for MmuPV1 genomic DNA (note serial sections in panels C and E for comparison); (G) IF for MmuPV1 L1 protein (green) and keratin 14 (red). The brightness of the photos in panel G was enhanced equivalently to better illustrate L1 staining. (B, D, F, H) Morphometric quantification of each tumor section (vehicle, V; 15 mg/ml cobimetinib, C; 2.0 mg/kg trametinib, T) on raw images (n = 5-6/group) for the percent of MPO positive cells in the tumor (B), region of positive E6/E7 ISH staining per mm of papilloma (D), region of positive LCR ISH staining per mm of papilloma (F), and number of L1 positive foci per tumor (H). Data were analyzed using one-way ANOVA with Tukey's multiple comparison test (*$p<0.05$, **$p<0.01$).

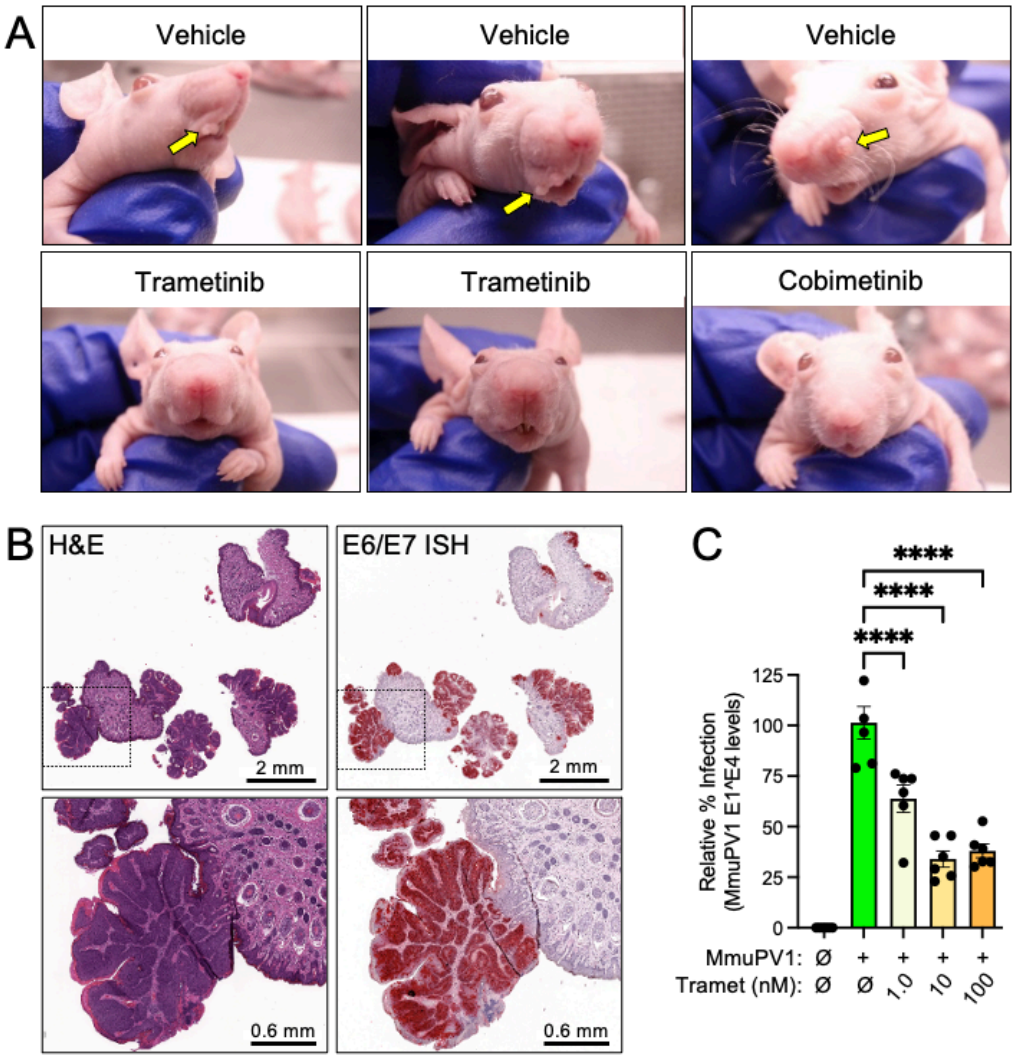

Figure 4. MEK inhibition provides protection against MmuPV1 transmission to secondary epithelial sites. (A) Mice that were co-housed throughout the 30-day treatment period; arrows indicate papillomas that developed on the muzzles of vehicle-treated mice. (B) Histological images of facial papillomas harvested on day 30 post treatment. Tissue sections were stained with H&E or by MmuPV1 E6/E7 ISH. Smaller boxes in upper panels indicate regions of increased magnification (lower panels). (C) Relative MmuPV1 infection in untreated cells compared to those treated with increasing concentrations of trametinib. Data summarize three independent infections analyzed by one-way ANOVA with Dunnett's multiple comparisons test (**** $p<0.0001$).

481 **TABLES**

482

483 **Table 1. Summary of animals developing visible muzzle warts**

Group	Wart positive mice / group total	Percentage
Vehicle	6/6	100%
7.5 mg/kg Cobimetinib	1/6	16.7%
15 mg/kg Cobimetinib	0/6	0%
1.0 mg/kg Trametinib	0/6	0%
2.0 mg/kg Trametinib	0/6	0%

484

485 **Supplementary Information**

486 Supplementary Figures

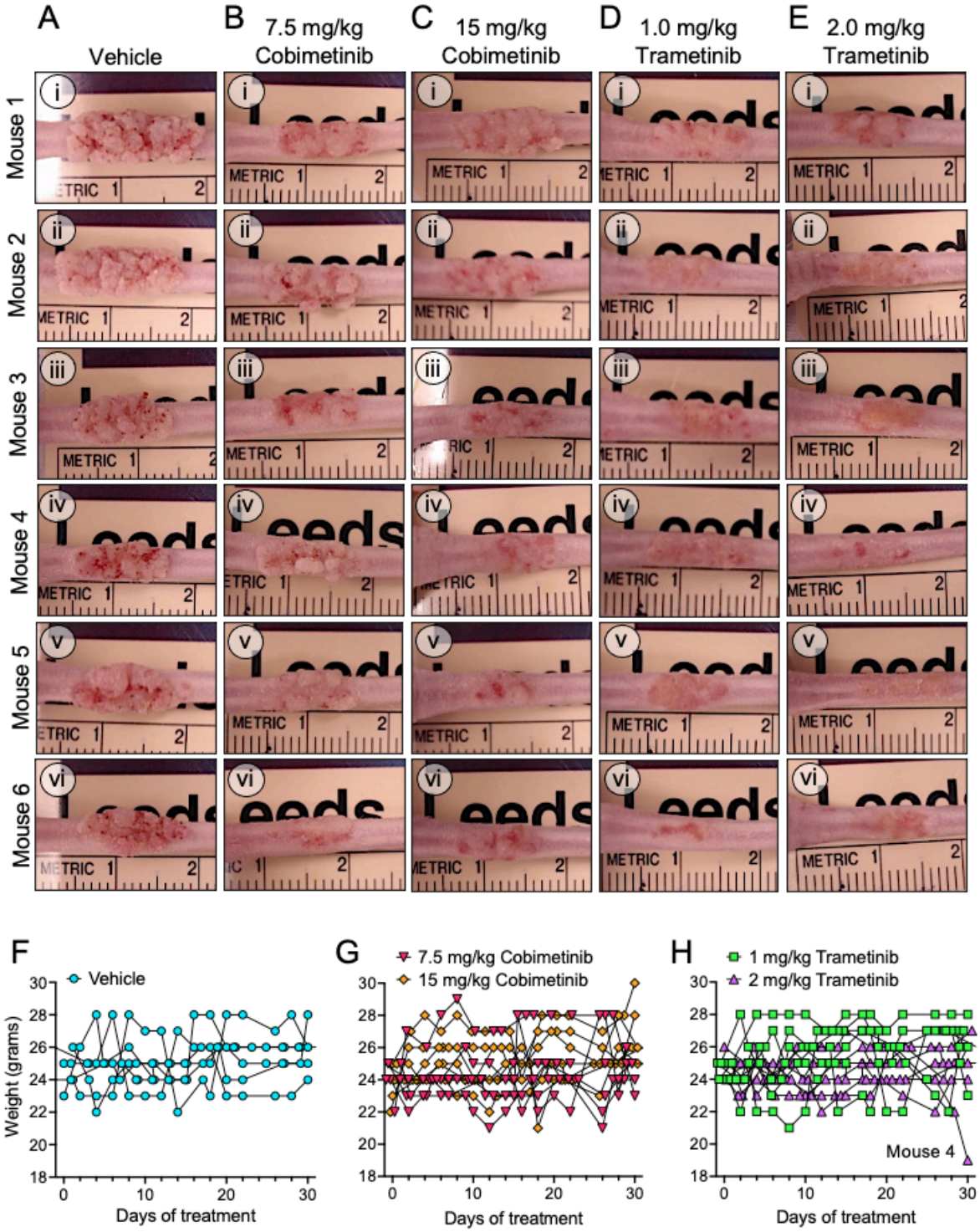

487

488 **Supplemental Information Fig. S1.** Visual phenotypes of MmuPV1-induced papillomas at day 32 post treatment
489 (prior to harvest). MmuPV1-induced papillomas after treatment with vehicle (A), 7.5 mg/kg cobimetinib (B), 15
490 mg/kg cobimetinib (C), 1 mg/kg trametinib (D), or 2 mg/kg trametinib (E). The labels at the left identify animal
491 numbers in each treatment group. (F-H) Mouse weights during treatment period. Note that only one animal (mouse
492 4 of the 2 mg/kg trametinib treatment arm) showed substantial weight loss (>20% of starting weight).

493

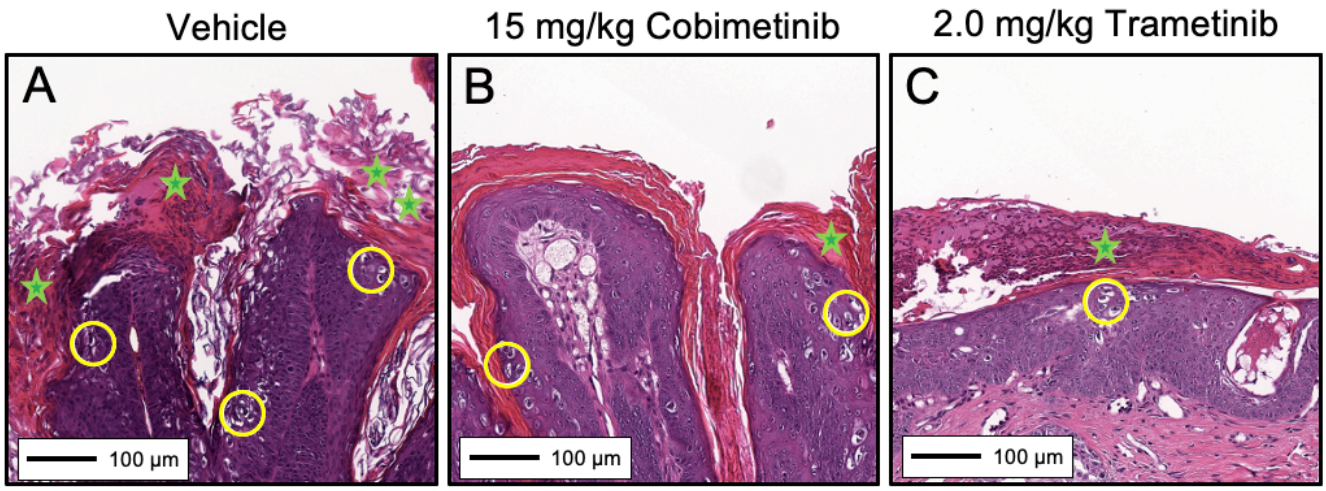

494

495 **Supplemental Information Fig. S2. Histologic features of MmuPV1-induced papillomas**. High-magnification
496 images of H&E-stained papillomatous tissue sections from animals treated with vehicle (A), 15 mg/kg cobimetinib
497 (B) or 2.0 mg/kg trametinib (C). Regions of hyperkeratosis are denoted with green stars. Koilocytes, a hallmark of
498 papillomavirus infections, are encircled in yellow.

499

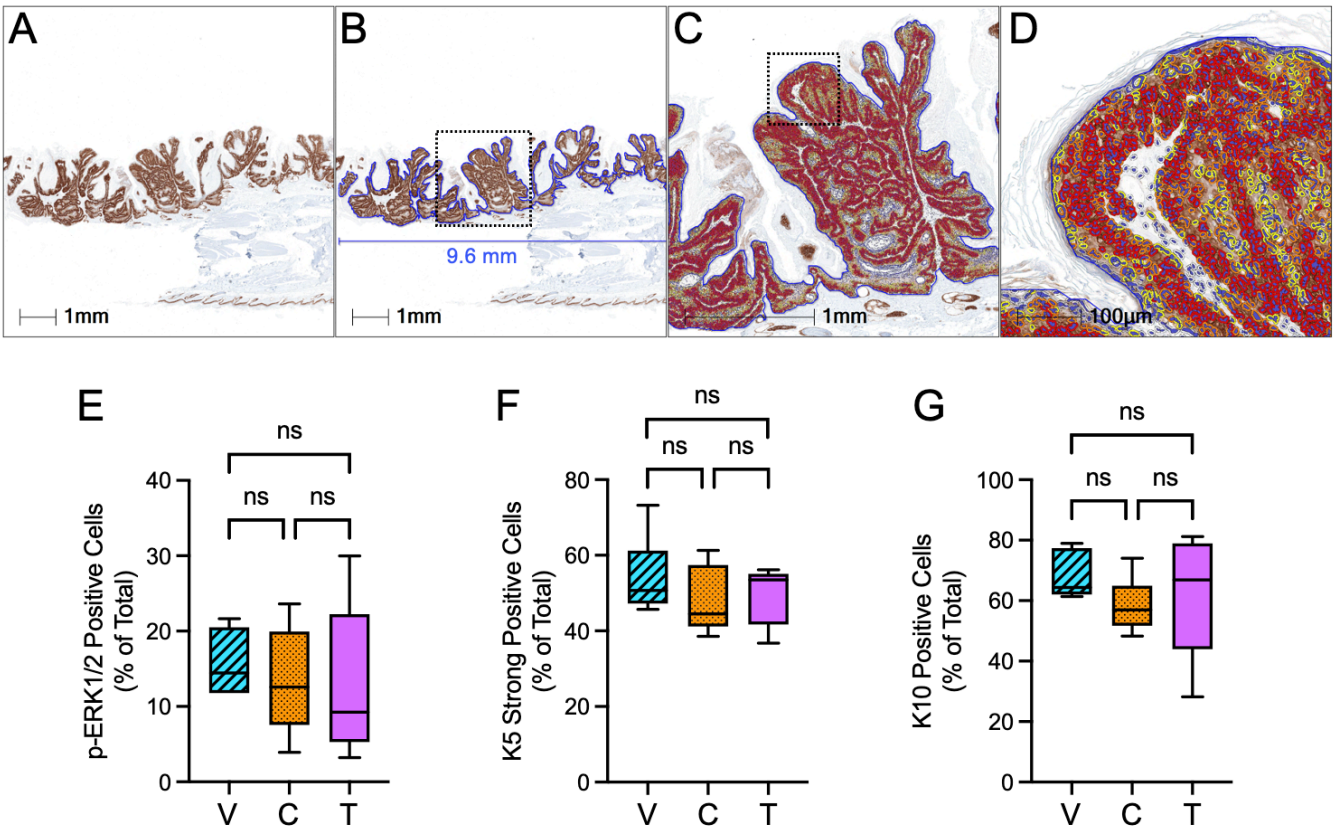

Supplemental Information Fig. S3. Example of pathologist-guided morphometric analysis using a HALO algorithm to identify and quantify the areas of strong positive K5 staining and comparisons of % biomarker signals amongst the tumor groups. (A-B) Tumor-bearing areas were selected (blue) and defined as nuclei-containing epithelium; the boxed area in B was subject to increased magnification in panel C. (C) Using the CytoNuclear algorithm, individual epithelial cells were identified *via* marking nuclei blue and cytoplasmic staining for each marker was categorized as negative (clear), low (yellow), medium (orange), or high (red). (D) Increased magnification of the boxed area in panel C. Because cells gradually loose K5 expression as they begin to differentiate and express K10, only the strong K5 positive cells were enumerated. (E-G) Summary of morphometric analyses for the percentage of MmuPV1-induced tumors cells expressing the cellular proteins p-ERK1/2 (E), strong K5 (F), and K10 (G) for mice treated with vehicle (V), 15 mg/ml cobimetinib (C), 2 mg/kg trametinib (T). Data were analyzed using one-way ANOVA with Tukey's multiple comparison test (ns = not significant).

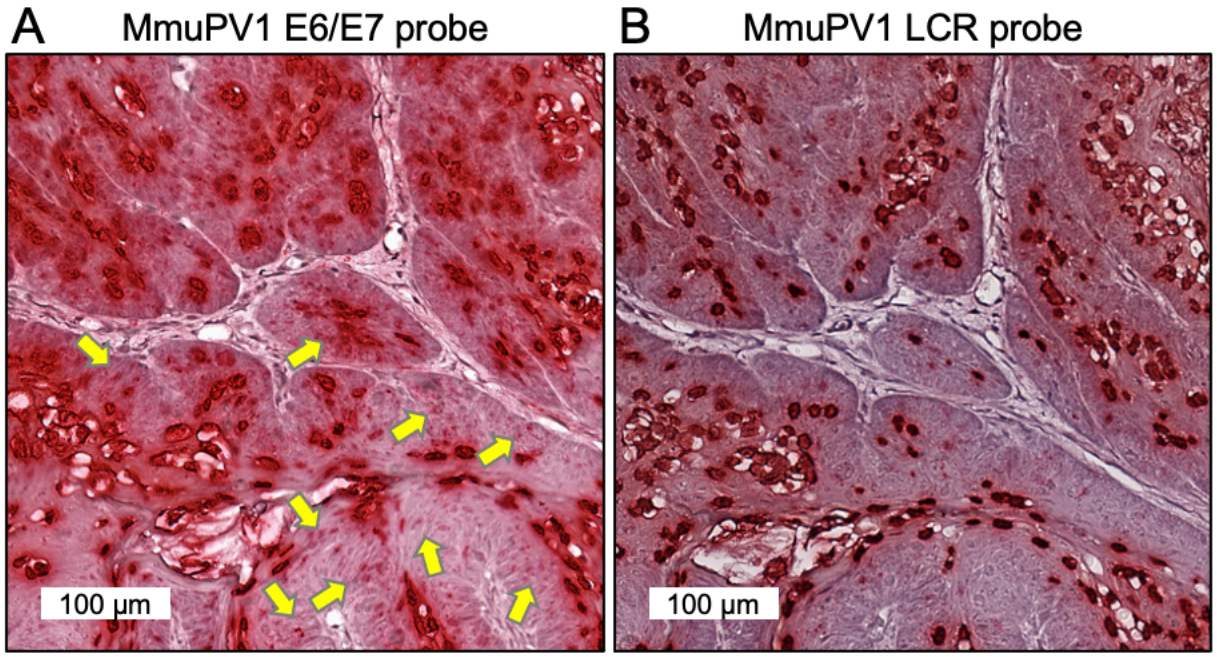

516

517 **Supplemental Information Fig. S4. Magnified images of ISH using probes specific for the MmuPV1 E6/E7**
518 **coding region (A) and the noncoding genomic LCR segment (B) in adjacent tumor sections from a**
519 **vehicle-treated mouse.** Note that both probes strongly stained nuclei in koilocytes and suprabasal cells likely to
520 be amplifying viral genomes. Whereas the E6/E7 probes demonstrated cytoplasmic punctate signals expected for
521 viral mRNAs (A, yellow arrows), the LCR probe produced little cytoplasmic signal (B).

522

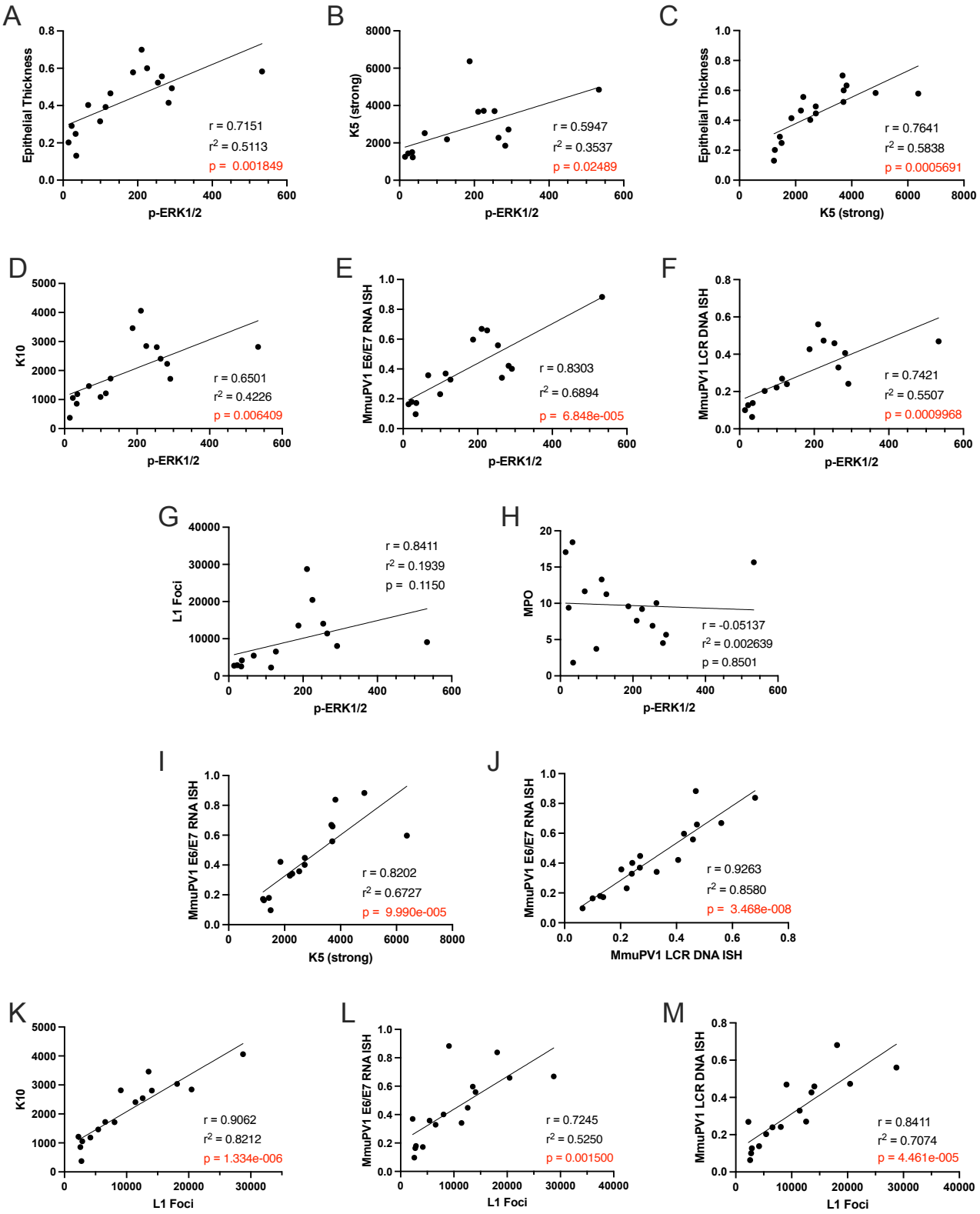

Supplemental Information Fig. S5. MEK inhibitor reduced tissue levels of p-ERK1/2 correlate with cellular and viral biomarkers in MmuPV1-induced tail tumors. Scatter dot plot correlations analyses between selected biomarkers were calculated using Pearson correlation coefficient (r) analysis and two-tailed (p values).

528

529 **SI Table 1. Mean and Standard Error (SE) of Tumor Volumes (mm^3)**

Time (days)	**Vehicle** Mean (SE)	**7.5 mg/kg Cobimetinib** Mean (SE)	**15 mg/kg Cobimetinib** Mean (SE)	**1.0 mg/kg Trametinib** Mean (SE)	**2.0 mg/kg Trametinib** Mean (SE)	**p-value[a]**
0	39.2 (8.1)	39.8 (6.3)	40.8 (6.3)	39.3 (8.0)	41.6 (7.5)	0.998996
2	46.8 (7.1)	42.1 (5.4)	48 (11.6)	40.1 (6.1)	46.1 (7.5)	0.906252
4	56.1 (9.0)	42.6 (5.8)	41.9 (7.9)	31.1 (5.5)	37.8 (8.7)	0.20922
6	61.2 (12.8)	47.0 (4.4)	41.1 (6.0)	40.9 (8.3)	34.3 (6.3)	0.27487
8	65.8 (11.6)	41.5 (7.5)	33.5 (9.2)	30.9 (5.9)	25.5 (4.3)	0.041988
10	65.8 (11.2)	34.9 (5.9)	37.8 (8.3)	29.5 (5.1)	26.0 (5.4)	0.069824
12	78.9 (12.2)	36.9 (4.6)	35.5 (9.3)	29.1 (7.7)	24.5 (6.0)	0.023779
14	84.5 (10.6)	40.3 (5.7)	36.0 (9.2)	24.1 (4.0)	25.9 (6.2)	0.001759
16	82.9 (16.0)	38.5 (5.3)	35.7 (11)	23.5 (4.4)	20.9 (4.4)	0.005515
18	92.3 (16.0)	34.0 (6.6)	32.7 (9.5)	30.3 (3.7)	21.8 (4.3)	0.016097
20	80.7 (17.1)	38.3 (6.9)	39.0 (10.7)	24.8 (5.1)	22.4 (3.7)	0.015508
22	84.7 (17.3)	43.2 (6.2)	40.0 (10.0)	24.4 (4.5)	20.7 (6.1)	0.004064
24	95.2 (22.1)	44.4 (7.3)	37.7 (9.8)	22.5 (2.6)	21.4 (4.5)	0.004354
28	109.2 (19.2)	51.4 (10.7)	36.4 (8.8)	22.6 (4.6)	23.2 (5.8)	0.002729
30	101.7 (19.1)	42.4 (8.0)	45.4 (13.2)	25.0 (4.4)	25.2 (4.8)	0.00718

530
531 [a] p-value for the significance of the difference in tumor volume among the five groups obtained using GLS to
532 account for unequal variances.
533

534 **SI Table 2. Pairwise Comparisons of Final Tumor Volumes Among Treatment Groups at 30 Days of**
535 **Treatment**

Treatment 1	Treatment 2	Difference[a]	Lower[b]	Upper[c]	p-value adj[d]
1.0 mg/kg Trametinib	Vehicle	-76.7042163	-88.255000	-65.15343	0.0005834
2.0 mg/kg Trametinib	Vehicle	-76.4767450	-88.027529	-64.92596	0.0006047
7.5 mg/kg Cobimetinib	Vehicle	-59.2767633	-70.827547	-47.72598	0.0087560
15 mg/kg Cobimetinib	Vehicle	-56.2683900	-67.819174	-44.71761	0.0137132
2.0 mg/kg Trametinib	1.0 mg/kg Trametinib	0.2274713	-11.323313	11.77826	1.0000000
7.5 mg/kg Cobimetinib	1.0 mg/kg Trametinib	17.4274530	5.876669	28.97824	0.8121645
15 mg/kg Cobimetinib	1.0 mg/kg Trametinib	20.4358263	8.885042	31.98661	0.7095422
7.5 mg/kg Cobimetinib	2.0 mg/kg Trametinib	17.1999817	5.649198	28.75077	0.8192129
15 mg/kg Cobimetinib	2.0 mg/kg Trametinib	20.2083550	8.657571	31.75914	0.7178020
15 mg/kg Cobimetinib	7.5 mg/kg Cobimetinib	3.0083733	-8.542411	14.55916	0.9997039

536
537 [a] The difference in tumor volumes between the pair of the groups
538 [b] The lower bounds of the 95% confidence interval (CI)
539 [c] The upper bounds of the 95% confidence interval (CI)
540 [d] The adjusted p-value for testing the significance of the difference between the two treatments in columns one
541 and two. The results indicate that the difference between Vehicle and each of the groups with the MEK inhibitor
542 is significant (adj. p-value < 0.05). But there is no significant difference when comparing between any of the
543 groups that received the MEK inhibitor, as none of the corresponding p-values is less than 0.05.
544
545

546

547 **SI Table 3. Estimates for Rates of Change of Tumor Volumes (Slope)**

Group	Estimate[a]	SE[b]	DF[c]	t-value[d]	p-value[e]
Vehicle	1.849	0.615	445	3.01	0.0028
1 mg/kg Trametinib	-0.4739	0.2262	445	-2.09	0.0368
2 mg/kg Trametinib	-0.5325	0.254	445	-2.1	0.0366
7.5 mg/kg Cobimetinib	0.1011	0.2795	445	0.36	0.7178
15 mg/kg Cobimetinib	0.1168	0.3679	445	0.32	0.7509

548
549 [a] Estimates for the rate of change (mm^3/day) derived from the slopes of the linear equations
550 [b] The standard error (SE)
551 [c] The degree of freedom (DF)
552 [d] The value of t-test (t-value) where the t-test investigates whether the corresponding slopes are zero.
553 [e] The p-value investigates whether the rate of change significantly differs from zero.
554

555 SI Table 3 shows the estimates for the rate of change (mm^3/day), the slopes of the linear equations of the five
556 groups, along with the SE, DF, t-value and p-value. The t-test here investigates whether the corresponding slopes
557 are zero. The p-values in the first three rows are all smaller than 0.05, suggesting that the rate of change of
558 tumors in the vehicle-treated mice and of tumors in mice treated with trametinib significantly differ from zero. The
559 tumor volumes in vehicle-treated mice significantly increased over time (because the corresponding slope is
560 positive), and that of groups treated with trametinib significantly decreased over time (as the corresponding slopes
561 are negative). The tumor volumes in groups treated with cobimetinib have the smallest estimates for the slopes
562 (in the sense of the absolute value), and the corresponding p-values are very large, indicating that the rate of
563 change is not significantly different from zero (i.e., the tumor volumes, on average, did not have a significant
564 change over time).

565 **SI Table 4. Difference in Rates of Change of Tumor Volumes (Slope)**

Difference in Rate of Change	**Estimate[a]**	**SE[b]**	**DF[c]**	**t-value[d]**	**p-value[e]**
Between Vehicle and 1 mg/kg Trametinib	2.3229	0.6553	445	3.54	0.0004
Between Vehicle and 2 mg/kg Trametinib	2.3816	0.6654	445	3.58	0.0004
Between Vehicle and 7.5 mg/kg Cobimetinib	1.7479	0.6756	445	2.59	0.01
Between Vehicle and 15 mg/kg Cobimetinib	1.7322	0.7167	445	2.42	0.016
Between Vehicle and Overall Treatment	2.0462	0.6315	445	3.24	0.0013
Between Two Doses of Trametinib	0.05866	0.3402	445	0.17	0.8631
Between Two Doses of Cobimetinib	-0.01576	0.462	445	-0.03	0.9728
Between Trametinib and Cobimetinib	-0.6122	0.2869	445	-2.13	0.0334

566
567 [a] Estimates for difference in the rate of change (mm^3/day) between the two groups of interest obtained based on
568 the LMM
569 [b] The standard error (SE)
570 [c] The degree of freedom (DF)
571 [d] The value of t-test (t-value) where the t-test investigates whether the corresponding differences are zero.
572 [e] The p-value investigates whether the rate of change significantly differs between the groups of interest.
573

574 SI Table 4 shows the analysis of the individual tumor rates of change for each treatment group using the linear
575 mixed-effects model (LMM). Based on the fitted LMM, we estimated the differences in the rate of change for
576 comparisons of interest. The first four rows provide the estimates for the difference in the rate of change between
577 the Vehicle and each MEK inhibitor treatment group. The fact that the p-values are smaller than 0.05 indicates
578 that the rate of change differs significantly between each pair of the groups. The fifth row shows the comparison
579 between the Vehicle and overall treatment group (the union of all the treatment groups), and a small p-value
580 implies that the difference in the rate of change is significant. These results provide statistical evidence for the
581 considerable effect of MEK inhibitors on tumor growth. In rows six and seven, we compared the dose effect on
582 the rate of change among the same drug, and the large p-values indicate that the dose effect is insignificant.
583 Lastly, we compared the difference in the rate of change between the two drugs regardless of the dose. The
584 result indicates a significant difference in the rate of change between those treated with the two drugs (p-value =
585 0.0334).

586

587

588 **References**

589 1. Egawa, N., K. Egawa, H. Griffin, and J. Doorbar, *Human Papillomaviruses; Epithelial Tropisms,*
590 *and the Development of Neoplasia.* Viruses, 2015. **7**(7): p. 3863-3890.

591 2. *PaVE: Papillomavirus Episteme. Available online: http://pave.niaid.nih.gov/.* [cited (accessed
592 on 3 February 2023).

593 3. de Martel, C., M. Plummer, J. Vignat, and S. Franceschi, *Worldwide burden of cancer*
594 *attributable to HPV by site, country and HPV type.* Int. J. Cancer, 2017. **141**(4): p. 664-670.

595 4. Beachler, D.C., A.R. Kreimer, M. Schiffman, R. Herrero, S. Wacholder, A.-C. Rodriguez, et al.,
596 *Multisite HPV16/18 Vaccine Efficacy Against Cervical, Anal, and Oral HPV Infection.* J Natl
597 Cancer Inst, 2016. **108**(1).

598 5. Johnson, D.E., B. Burtness, C.R. Leemans, V.W.Y. Lui, J.E. Bauman, and J.R. Grandis, *Head*
599 *and neck squamous cell carcinoma.* Nat Rev Dis Prim, 2020. **6**(1): p. 92-22.

600 6. Maiman, M., *Management of cervical neoplasia in human immunodeficiency virus-infected*
601 *women.* J Natl Cancer Inst Monographs, 1998. **1998**(23): p. 43-49.

602 7. Martin, D., P. Balermpas, R. Winkelmann, F. Rödel, C. Rödel, and E. Fokas, *Anal squamous*
603 *cell carcinoma - State of the art management and future perspectives.* Cancer Treat Rev, 2018.
604 **65**: p. 11-21.

605 8. Stern, P.L., S.H. van der Burg, I.N. Hampson, T.R. Broker, A. Fiander, C.J. Lacey, et al.,
606 *Therapy of human papillomavirus-related disease.* Vaccine, 2012. **30 Suppl 5**: p. F71-82.

607 9. Ouda, A.M., A.A. Elsabagh, I.M. Elmakaty, I. Gupta, S. Vranic, H. Al-Thawadi, et al., *HPV and*
608 *Recurrent Respiratory Papillomatosis: A Brief Review.* Life (Basel, Switzerland), 2021. **11**(11):
609 p. 1279.

610 10. Oren-Shabtai, M., I. Snast, M. Lapidoth, S. Sherman, Y. Noyman, D. Mimouni, et al., *Topical*
611 *and Systemic Retinoids for the Treatment of Genital Warts: A Systematic Review and Meta-*
612 *Analysis.* Dermatology (Basel, Switzerland), 2021. **237**(3): p. 389-395.

613 11. Christensen, N.D., L.R. Budgeon, N.M. Cladel, and J. Hu, *Recent advances in preclinical model*
614 *systems for papillomaviruses.* Virus research, 2017. **231**: p. 108-118.

615 12. Spurgeon, M.E. and P.F. Lambert, *Mus musculus Papillomavirus 1: A New Frontier in Animal*
616 *Models of Papillomavirus Pathogenesis.* J. Virol., 2020. **94**(9): p. e00002-20.

617 13. Egawa, N. and J. Doorbar, *The low-risk papillomaviruses.* Virus Res., 2017. **231**: p. 119-127.

618 14. McBride, A.A., *Human papillomaviruses: diversity, infection and host interactions.* Nat Rev
619 Microbiol, 2021. **doi: 10.1038/s41579-021-00617-5**.

620 15. Doorbar, J., W. Quint, L. Banks, I.G. Bravo, M. Stoler, T.R. Broker, et al., *The biology and life-*
621 *cycle of human papillomaviruses.* Vaccine, 2012. **30 Suppl 5**: p. F55-70.

622 16. Meyers, J.M., A. Uberoi, M. Grace, P.F. Lambert, and K. Munger, *Cutaneous HPV8 and*
623 *MmuPV1 E6 Proteins Target the NOTCH and TGF-beta Tumor Suppressors to Inhibit*
624 *Differentiation and Sustain Keratinocyte Proliferation.* PLoS Pathog, 2017. **13**(1).

625 17. Hoppe-Seyler, K., F. Bossler, J.A. Braun, A.L. Herrmann, and F. Hoppe-Seyler, *The HPV E6/E7*
626 *Oncogenes: Key Factors for Viral Carcinogenesis and Therapeutic Targets.* Trends in
627 microbiology, 2018. **26**(2): p. 158-168.

628 18. Pal, A. and R. Kundu, *Human Papillomavirus E6 and E7: The Cervical Cancer Hallmarks and*
629 *Targets for Therapy.* Front Microbiol, 2019. **10**: p. 3116.

630 19. Goodwin, E. and D. DiMaio, *Repression of human papillomavirus oncogenes in HeLa cervical*
631 *carcinoma cells causes the orderly reactivation of dormant tumor suppressor pathways.* Proc.
632 Natl. Acad. Sci., 2000. **97**(23): p. 12513-12518.

633 20. Horner, S.M., R.A. DeFilippis, L. Manuelidis, and D. DiMaio, *Repression of the Human*
634 *Papillomavirus E6 Gene Initiates p53-Dependent, Telomerase-Independent Senescence and*
635 *Apoptosis in HeLa Cervical Carcinoma Cells.* J. Virol., 2004. **78**(8): p. 4063-4073.

636 21. Rampias, T., C. Sasaki, P. Weinberger, and A. Psyrri, *E6 and E7 gene silencing and*
637 *transformed phenotype of human papillomavirus 16-positive oropharyngeal cancer cells.* J. Natl.
638 Cancer Inst., 2009. **101**(6): p. 412-423.

639 22. Zhou, J., B. Li, C. Peng, F. Wang, Z. Fu, C. Zhou, et al., *Inhibition of cervical cancer cell growth*
640 *in vitro and in vivo by lentiviral-vector mediated shRNA targeting the common promoter of*
641 *HPV16 E6 and E7 oncogenes.* Antiviral Res., 2013. **98**(2): p. 305-313.

642 23. Lee, C.J., E.J. Suh, H.T. Kang, J.S. Im, S.J. Um, J.S. Park, et al., *Induction of senescence-like*
643 *state and suppression of telomerase activity through inhibition of HPV E6/E7 gene expression in*
644 *cells immortalized by HPV16 DNA.* Exp. Cell Res., 2002. **277**(2): p. 173-182.

645 24. von Knebel Doeberitz, M., C. Rittmüller, H. zur Hausen, and M. Dürst, *Inhibition of*
646 *tumorigenicity of cervical cancer cells in nude mice by HPV E6-E7 anti-sense RNA.* Int. J.
647 Cancer, 1992. **51**(5): p. 831-834.

648 25. Sima, N., S. Wang, W. Wang, D. Kong, Q. Xu, X. Tian, et al., *Antisense targeting human*
649 *papillomavirus type 16 E6 and E7 genes contributes to apoptosis and senescence in SiHa*
650 *cervical carcinoma cells.* Gynecol Oncol, 2007. **106**(2): p. 299-304.

651 26. Sima, N., W. Wang, D. Kong, D. Deng, Q. Xu, J. Zhou, et al., *RNA interference against HPV16*
652 *E7 oncogene leads to viral E6 and E7 suppression in cervical cancer cells and apoptosis via*
653 *upregulation of Rb and p53.* Apoptosis, 2008. **13**(2): p. 273-281.

654 27. Kennedy, E.M., A.V.R. Kornepati, M. Goldstein, H.P. Bogerd, B.C. Poling, A.W. Whisnant, et al.,
655 *Inactivation of the human papillomavirus E6 or E7 gene in cervical carcinoma cells by using a*
656 *bacterial CRISPR/Cas RNA-guided endonuclease.* J. Virol., 2014. **88**(20): p. 11965-11972.

657 28. Zheng, K., N. Egawa, A. Shiraz, M. Katakuse, M. Okamura, H.M. Griffin, et al., *The Reservoir of*
658 *Persistent Human Papillomavirus Infection; Strategies for Elimination Using Anti-Viral*
659 *Therapies.* Viruses, 2022. **14**(2): p. 214.

660 29. Luna, A.J., R.T. Sterk, A.M. Griego-Fisher, J.-Y. Chung, K.L. Berggren, V. Bondu, et al.,
661 *MEK/ERK Signaling is a Critical Regulator of High-Risk Human Papillomavirus Oncogene*
662 *Expression Revealing Therapeutic Targets for HPV-Induced Tumors.* PLoS Pathog, 2021.
663 **17**(1): p. e1009216.

664 30. Samatar, A.A. and P.I. Poulikakos, *Targeting RAS-ERK signalling in cancer: promises and*
665 *challenges.* Nat Rev Drug Discov, 2014. **13**(12): p. 928-42.

666 31. Curto, M., B.K. Cole, D. Lallemand, C.-H. Liu, and A.I. McClatchey, *Contact-dependent*
667 *inhibition of EGFR signaling by Nf2/Merlin.* J. Cell Biol., 2007. **177**(5): p. 893-903.

668 32. McClatchey, A.I. and A.S. Yap, *Contact inhibition (of proliferation) redux.* Curr Opin Cell Biol,
669 2012. **24**(5): p. 685-694.

670 33. Scholl, F.A., P.A. Dumesic, D.I. Barragan, K. Harada, V. Bissonauth, J. Charron, et al., *Mek1/2*
671 *MAPK Kinases Are Essential for Mammalian Development, Homeostasis, and Raf-Induced*
672 *Hyperplasia.* Dev Cell, 2007. **12**(4): p. 615-629.

673 34. Cursons, J., J. Gao, D.G. Hurley, C.G. Print, P.R. Dunbar, M.D. Jacobs, et al., *Regulation of*
674 *ERK-MAPK signaling in human epidermis.* BMC systems biology, 2015. **9**: p. 41-41.

675 35. Shaul, Y.D. and R. Seger, *The MEK/ERK cascade: from signaling specificity to diverse*
676 *functions.* Biochim. Biophys. Acta., 2007. **1773**(8): p. 1213-1226.

677 36. Catalanotti, F., G. Reyes, V. Jesenberger, G. Galabova-Kovacs, R. de Matos Simoes, O.
678 Carugo, et al., *A MEK1-MEK2 heterodimer determines the strength and duration of the ERK*
679 *signal.* Nat Struct Mol Biol, 2009. **16**(3): p. 294-303.

680 37. Brunet, A., G. Pagès, and J. Pouysségur, *Growth factor-stimulated MAP kinase induces rapid*
681 *retrophosphorylation and inhibition of MAP kinase kinase (MEK1).* FEBS Lett, 1994. **346**(2-3): p.
682 299-303.

683 38. Xu, B., J.L. Wilsbacher, T. Collisson, and M.H. Cobb, *The N-terminal ERK-binding site of MEK1*
684 *is required for efficient feedback phosphorylation by ERK2 in vitro and ERK activation in vivo.* J
685 Biol Chem, 1999. **274**(48): p. 34029-35.

686 39. Schaeffer, H.J., A.D. Catling, S.T. Eblen, L.S. Collier, A. Krauss, and M.J. Weber, *MP1: a MEK*
687 *binding partner that enhances enzymatic activation of the MAP kinase cascade.* Science, 1998.
688 **281**(5383): p. 1668-71.

689 40. Kolch, W., *Coordinating ERK/MAPK signalling through scaffolds and inhibitors.* Nat Rev Mol
690 Cell Biol, 2005. **6**(11): p. 827-37.

691 41. Roy, M., Z. Li, and D.B. Sacks, *IQGAP1 is a scaffold for mitogen-activated protein kinase*
692 *signaling.* Mol Cell Biol, 2005. **25**(18): p. 7940-52.

693 42. Yin, G., J. Haendeler, C. Yan, and B.C. Berk, *GIT1 functions as a scaffold for MEK1-*
694 *extracellular signal-regulated kinase 1 and 2 activation by angiotensin II and epidermal growth*
695 *factor.* Mol Cell Biol, 2004. **24**(2): p. 875-85.

696 43. Liang, R.-Y., B.-H. Liu, C.-J. Huang, K.-T. Lin, C.-C. Ko, L.-L. Huang, et al., *MEK2 is a critical*
697 *modulating mechanism to down-regulate GCIP stability and function in cancer cells.* The FASEB
698 Journal, 2020. **34**(2): p. 1958-1969.

699 44. Giroux, S., M. Tremblay, D. Bernard, J.F. Cardin-Girard, S. Aubry, L. Larouche, et al.,
700 *Embryonic death of Mek1-deficient mice reveals a role for this kinase in angiogenesis in the*
701 *labyrinthine region of the placenta.* Curr Biol, 1999. **9**(7): p. 369-72.

702 45. Bélanger, L.F., S. Roy, M. Tremblay, B. Brott, A.M. Steff, W. Mourad, et al., *Mek2 is*
703 *dispensable for mouse growth and development.* Mol Cell Biol, 2003. **23**(14): p. 4778-87.

704 46. Cho, H., J.-Y. Chung, K.-H. Song, K.H. Noh, B.W. Kim, E.J. Chung, et al., *Apoptosis inhibitor-5*
705 *overexpression is associated with tumor progression and poor prognosis in patients with*
706 *cervical cancer.* BMC Cancer, 2014. **14**(1): p. 545.

707 47. Wang, W.-M., S.-Y. Wu, A.-Y. Lee, and C.-M. Chiang, *Binding site specificity and factor*
708 *redundancy in activator protein-1-driven human papillomavirus chromatin-dependent*
709 *transcription.* J. Biol. Chem., 2011. **286**(47): p. 40974-40986.

710 48. Cheng, Y. and H. Tian, *Current Development Status of MEK Inhibitors.* Molecules (Basel,
711 Switzerland), 2017. **22**(10): p. 1551.

712 49. Egawa, N., A. Shiraz, R. Crawford, T. Sanders-Wood, J. Yarwood, M. Rogers, et al., *Dynamics*
713 *of Papillomavirus In Vivo Disease Formation & Susceptibility to High-level Disinfection.*
714 *Implications for Transmission in Clinical Settings.* EBioMedicine, 2021. **63**: p. 103177.

715 50. Young, J.M., A. Zine El Abidine, R.A. Gómez-Martinez, V. Bondu, R.T. Sterk, Z. Surviladze, et
716 al., *Protamine Sulfate Is a Potent Inhibitor of Human Papillomavirus Infection In Vitro and in*
717 *Vivo.* Antimicrobial Agents and Chemotherapy, 2022. **66**(1): p. e01513-21.

718 51. Reid, R., C.P. Crum, B.R. Herschman, Y.S. Fu, L. Braun, K.V. Shah, et al., *Genital warts and*
719 *cervical cancer. III. Subclinical papillomaviral infection and cervical neoplasia are linked by a*
720 *spectrum of continuous morphologic and biologic change.* Cancer, 1984. **53**(4): p. 943-53.

721 52. Khavari, T.A. and J. Rinn, *Ras/Erk MAPK signaling in epidermal homeostasis and neoplasia.*
722 Cell Cycle, 2007. **6**(23): p. 2928-31.

723 53. Alam, H., L. Sehgal, S.T. Kundu, S.N. Dalal, and M.M. Vaidya, *Novel function of keratins 5 and*
724 *14 in proliferation and differentiation of stratified epithelial cells.*, in *Mol Biol Cell*. 2011,
725 American Society for Cell Biology. p. 4068-4078.

726 54. Zhang, L.-j., *Keratins in Skin Epidermal Development and Diseases*, in *Keratin*, M. Blumenberg,
727 Editor. 2018, IntechOpen: London. p. 10.5772/intechopen.79050.

728 55. Sundberg, J.P., T.M. Stearns, J. Joh, M. Proctor, A. Ingle, K.A. Silva, et al., *Immune status,*
729 *strain background, and anatomic site of inoculation affect mouse papillomavirus (MmuPV1)*
730 *induction of exophytic papillomas or endophytic trichoblastomas.* PLoS ONE, 2014. **9**(12): p.
731 e113582.

732 56. Spurgeon, M.E., A. Uberoi, S.M. McGregor, T. Wei, E. Ward-Shaw, and P.F. Lambert, *A Novel*
733 *In Vivo Infection Model To Study Papillomavirus-Mediated Disease of the Female Reproductive*
734 *Tract.* mBio, 2019. **10**(2): p. 607.

735 57. Yilmaz, V., P. Louca, L. Potamiti, M. Panayiotidis, and K. Strati, *A novel lineage-tracing mouse*
736 *model for studying early MmuPV1 infections.* eLife, 2022. **11**: p. e72638.

737 58. Keating, J.T., A. Cviko, S. Riethdorf, L. Riethdorf, B.J. Quade, D. Sun, et al., *Ki-67, cyclin E, and*
738 *p16INK4 are complimentary surrogate biomarkers for human papilloma virus-related cervical*
739 *neoplasia.* Am J Surg Pathol, 2001. **25**(7): p. 884-91.

740 59. Gilmartin, A.G., M.R. Bleam, A. Groy, K.G. Moss, E.A. Minthorn, S.G. Kulkarni, et al.,
741 *GSK1120212 (JTP-74057) Is an Inhibitor of MEK Activity and Activation with Favorable*

742 *Pharmacokinetic Properties for Sustained In Vivo Pathway Inhibition.* Clin. Cancer Res., 2011.
743 **17**(5): p. 989-1000.

744 60. Liu, Y., R. Zhao, X. Qin, X. Mao, Q. Li, and S. Fang, *Cobimetinib Sensitizes Cervical Cancer to*
745 *Paclitaxel via Suppressing Paclitaxel-Induced ERK Activation.* Pharmacology, 2022. **107**(7-8): p.
746 398-405.

747 61. Gertych, A., S. Mohan, S. Maclary, S. Mohanty, K. Wawrowsky, J. Mirocha, et al., *Effects of*
748 *tissue decalcification on the quantification of breast cancer biomarkers by digital image analysis.*
749 Diagnostic Pathology, 2014. **9**(1): p. 213.

750 62. Coleman, N., H.D. Birley, A.M. Renton, N.F. Hanna, B.K. Ryait, M. Byrne, et al., *Immunological*
751 *events in regressing genital warts.* Am J Clin Pathol, 1994. **102**(6): p. 768-74.

752 63. Trimble, C.L., R.A. Clark, C. Thoburn, N.C. Hanson, J. Tassello, D. Frosina, et al., *Human*
753 *papillomavirus 16-associated cervical intraepithelial neoplasia in humans excludes CD8 T cells*
754 *from dysplastic epithelium.* J Immunol, 2010. **185**(11): p. 7107-14.

755 64. Woo, Y.L., J. Sterling, I. Damay, N. Coleman, R. Crawford, S.H. van der Burg, et al.,
756 *Characterising the local immune responses in cervical intraepithelial neoplasia: a cross-*
757 *sectional and longitudinal analysis.* Bjog, 2008. **115**(13): p. 1616-21; discussion 1621-2.

758 65. Handisurya, A., P.M. Day, C.D. Thompson, M. Bonelli, D.R. Lowy, and J.T. Schiller, *Strain-*
759 *Specific Properties and T Cells Regulate the Susceptibility to Papilloma Induction by Mus*
760 *musculus Papillomavirus 1.* PLoS Pathog., 2014. **10**(8): p. e1004314.

761 66. Cladel, N.M., L.R. Budgeon, K.K. Balogh, T.K. Cooper, S.A. Brendle, N.D. Christensen, et al.,
762 *Mouse papillomavirus infection persists in mucosal tissues of an immunocompetent mouse*
763 *strain and progresses to cancer.* Scientific reports, 2017. **7**(1): p. 16932-12.

764 67. Doorbar, J., *The papillomavirus life cycle.* J. Clin. Virol., 2005. **32S**: p. S7-S15.

765 68. Bernard, H.-U., *Regulatory elements in the viral genome.* Virology, 2013. **445**(1-2): p. 197-204.

766 69. Fuse, M.A., C.T. Dinh, J. Vitte, J. Kirkpatrick, T. Mindos, S.K. Plati, et al., *Preclinical*
767 *assessment of MEK1/2 inhibitors for neurofibromatosis type 2-associated schwannomas reveals*
768 *differences in efficacy and drug resistance development.* Neuro Oncol, 2019. **21**(4): p. 486-497.

769 70. Hoeflich, K.P., M. Merchant, C. Orr, J. Chan, D. Den Otter, L. Berry, et al., *Intermittent*
770 *administration of MEK inhibitor GDC-0973 plus PI3K inhibitor GDC-0941 triggers robust*
771 *apoptosis and tumor growth inhibition.* Cancer Res, 2012. **72**(1): p. 210-9.

772 71. Maglennon, G.A., P.B. McIntosh, and J. Doorbar, *Immunosuppression facilitates the reactivation*
773 *of latent papillomavirus infections.* J Virol, 2014. **88**(1): p. 710-6.

774 72. Dreyer, G., *Clinical implications of the interaction between HPV and HIV infections.* Best Pract
775 Res Clin Obstet Gynaecol, 2018. **47**: p. 95-106.

776 73. Doorbar, J., *Host control of human papillomavirus infection and disease.* Best Pract Res Clin
777 Obstet Gynaecol, 2018. **47**: p. 27-41.

778 74. Weiss, A. and D.R. Littman, *Signal transduction by lymphocyte antigen receptors.* Cell, 1994.
779 **76**(2): p. 263-274.

780 75. Nakayama, T. and M. Yamashita, *The TCR-mediated signaling pathways that control the*
781 *direction of helper T cell differentiation.* Seminars in Immunology, 2010. **22**(5): p. 303-309.

782 76. Lieske, N.V., K. Tonby, D. Kvale, A.M. Dyrhol-Riise, and K. Tasken, *Targeting Tuberculosis and*
783 *HIV Infection-Specific Regulatory T Cells with MEK/ERK Signaling Pathway Inhibitors.* PLoS
784 One, 2015. **10**(11): p. e0141903.

785 77. Verma, V., N. Jafarzadeh, S. Boi, S. Kundu, Z. Jiang, Y. Fan, et al., *MEK inhibition reprograms*
786 *CD8(+) T lymphocytes into memory stem cells with potent antitumor effects.* Nat Immunol, 2021.
787 **22**(1): p. 53-66.

788